Received: 1 June 2021 | Revised: 2 February 2022 | Accepted: 29 March 2022

DOI: 10.1002/jev2.12220

TECHNICAL REPORT

Contaminating transfection complexes can masquerade as small extracellular vesicles and impair their delivery of RNA

Jenna McCann[1] | **Carmen Daniela Sosa-Miranda**[1] | **Huishan Guo**[1] | **Ryan Reshke**[1] | **Alexandre Savard**[1] | **Adriana Zardini Buzatto**[2] | **James A. Taylor**[1] | **Liang Li**[2,3] | **Derrick J. Gibbings**[1,4,5]

[1]Department of Cellular and Molecular Medicine, University of Ottawa, Ottawa, Ontario, Canada

[2]The Metabolomics Innovation Centre, University of Alberta, Edmonton, Alberta, Canada

[3]Department of Chemistry, University of Alberta, Edmonton, Alberta, Canada

[4]Institute for Systems Biology, University of Ottawa, Ottawa, Ontario, Canada

[5]Faculty of Medicine, Eric Poulin Centre for Neuromuscular Disease, University of Ottawa, Ottawa, Ontario, Canada

Correspondence
Derrick Gibbings, Department of Cellular and Molecular Medicine, University of Ottawa, Ottawa, Ontario K1H 8M5, Canada.
Email: gibbings@uottawa.ca

Funding information
Natural Science and Engineering Research Council of Canada

Abstract

One of the functions of small extracellular vesicles (sEVs) which has received the most attention is their capacity to deliver RNA into the cytoplasm of target cells. These studies have often been performed by transfecting RNAs into sEV-producing cells, to later purify and study sEV delivery of RNA. Transfection complexes and other delivery vehicles accumulate in late endosomes where sEV are formed and over 50% of transfection complexes or delivery vehicles administered to cells are released again to the extracellular space by exocytosis. This raises the possibility that transfection complexes could alter sEVs and contaminate sEV preparations. We found that widely used transfection reagents including RNAiMax and INTERFERin accumulated in late endosomes. These transfection complexes had a size similar to sEV and were purified by ultracentrifugation like sEV. Focusing on the lipid-based transfection reagent RNAiMax, we found that preparations of sEV from transfected cells contained lipids from transfection complexes and transfected siRNA was predominantly in particles with the density of transfection complexes, rather than sEV. This suggests that transfection complexes, such as lipid-based RNAiMax, may frequently contaminate sEV preparations and could account for some reports of sEV-mediated delivery of nucleic acids. Transfection of cells also impaired the capacity of sEVs to deliver stably-expressed siRNAs, suggesting that transfection of cells may alter sEVs and prevent the study of their endogenous capacity to deliver RNA to target cells.

KEYWORDS

contaminant, delivery, endosomes, extracellular vesicles, lipid nanoparticles, RNA, therapeutics, transfection complexes

1 | INTRODUCTION

Cellular specialization is essential to most multicellular organisms and depends on the plasma membrane to limit the spread between cells of differentiation factors and the RNAs which encode and regulate them. Restricting the uncontrolled intercellular movement of nucleic acids is thus critical to complex animals and most multicellular organisms. Despite this, organisms have evolved ways to exchange RNA between cells in particular circumstances. For example, plants allow systemic movement of small RNA silencing signals to silence viral pathogens (Liu & Chen, 2018) and *C.elegans* exhibits uptake and systemic movement of ingested double-stranded RNAs (Fire et al., 1998). Mammals can use small extracellular vesicles (sEV) called exosomes to transfer

RNA between cells (Skog et al., 2008; Valadi et al., 2007). The scope of RNA transfer by sEV in development, disease and drug delivery is a subject of much investigation.

sEV are 50–150 nm vesicles surrounded by a lipid bilayer (Van Niel et al., 2018). sEV can be formed by inward budding of endosomal membranes to form multivesicular bodies (Van Niel et al., 2018). When these multivesicular bodies fuse with the plasma membrane, sEV are released into the extracellular space. sEV may also form by budding from the plasma membrane (Booth et al., 2006). Due to their biogenesis, the sEV surface is coated with proteins and receptors also found on the surface of cells and their lumen contains RNA and other molecules derived from the cytoplasm (Van Niel et al., 2018).

Studies of sEV are technically complex. As sEV are below the resolution limits of most light microscopes researchers necessarily rely on their defining physical and biochemical characteristics to demonstrate the presence and functions of sEVs (Théry et al., 2018). These sEV characteristics include a size of 50–150 nm, a density of 1.05–1.15 g/ml, and the presence of a lipid bilayer which protects their lumenal contents including RNA. Methods to purify sEV, including ultracentrifugation, tangential flow filtration and size selection columns rely on these characteristics. However, the presence of contaminants in preparations of sEV is widely acknowledged (Mateescu et al., 2017; Théry et al., 2018). These contaminants are far from completely understood but include lipid particles and protein complexes (Jeppesen et al., 2019; Takov et al., 2017). Contaminants like these raise a fundamental challenge to one's ability to conclude that functions observed in experiments are due to sEV (Takov et al., 2017), and not contaminants of sEV preparations. For example, some studies have used electroporation to putatively introduce RNA into sEVs and demonstrate the capacity of sEVs to deliver RNA to target cells (Alvarez-Erviti et al., 2011; Kamerkar et al., 2017; Usman et al., 2018). We, and others have provided evidence that electroporation of sEVs with RNA causes aggregation of RNA outside of sEVs and that this aggregated RNA copurifies with sEVs and has physical properties that can lead to the assumption that aggregated RNA is present inside of sEVs (Kooijmans et al., 2013; Reshke et al., 2020). This aggregated RNA outside of sEVs may account for some observations that electroporated sEVs deliver RNA to target cells.

The capacity to transiently introduce RNA and DNA into cells by transfection and related methods has become a mainstay of much biological research, and the foundation of new therapeutics using siRNA (ONPATTRO) (Adams et al., 2018), mRNA vaccines for COVID-19, and CRISPR gene editing (Gillmore et al., 2021). A wide array of strategies to introduce nucleic acids into cells have been used including lipid-based complexes (e.g., lipid nanoparticles (Hou et al., 2021)), many variations of polymers such as PEI (polyethylenimine) (Piotrowski-Daspit et al., 2020), and receptor-mediated uptake (e.g., GalNAc conjugates) (Akinc et al., 2010; Balwani et al., 2020; Klein et al., 2021). The common feature of nearly all these delivery or transfection strategies is uptake into acidic endosomal compartments (Brown et al., 2020; Hou et al., 2021; Piotrowski-Daspit et al., 2020; Rehman et al., 2013; Selby et al., 2017; Wittrup et al., 2015). Quantitative studies using lipid nanoparticles containing siRNA or GalNAC-conjugated siRNA in mice demonstrate that ~99% of the siRNA internalised by cells resides in endosomes (Brown et al., 2020; Gilleron et al., 2013; Pei et al., 2010; Wittrup et al., 2015), and less than 1% reaches the cytoplasm to effect mRNA silencing. For example, GalNAC-siRNA resides in acidic endosomes for weeks and treatment of mice with endolytic peptides weeks after siRNA treatment, boosts siRNA loading into Argonaute in the cytoplasm and target silencing (Brown et al., 2020). Because accumulation and entrapment in endosomes limits so drastically the efficacy of nucleic acid delivery with lipid, polymer, and ligand-based methods, engineering endosomal escape into delivery vehicles and transfection reagents has been a focus of much research for many years (Dowdy, 2017; Kanasty et al., 2013; Piotrowski-Daspit et al., 2020; Selby et al., 2017; Stewart et al., 2016).

Variations of polymer-, lipid- and ligand-based delivery vehicles used to deliver nucleic acid therapeutics in patients are used as transfection reagents in research labs. Lipid-based reagents such as Lipofectamine or Lipofectamine RNAiMax are examples of widely used transfection reagents. Lipid-based transfection reagents like this are frequently composed of the cationic lipid DOTAP (n1,2-dioleoyl-3-trimethylammonium-propane) and DOPE (,2-dioleoyl-sn-glycero-3- phosphoethanolamine) or related helper lipids. Like other lipid-based delivery vehicles, these accumulate in endosomes (Hui et al., 1996; Zelphati & Szoka, 1996) despite extensive efforts to optimize endosomal escape of nucleic acids.

Abundant in the endolysosomal system, transfection complexes may impact experiments with sEV through multiple pathways by breaking open endosomes (Van De Vyver et al., 2020; Wittrup et al., 2015), engaging repair pathways for the endosomal membrane (Du Rietz et al., 2020) and clogging the lumen of endolysosomal organelles (Jonker et al., 2017). Indeed, part of the toxicity of both transfection complexes and other nucleic acid delivery vehicles is believed to be due to disruption of endolysosomal function (Kanasty et al., 2012; Liu et al., 2021). Transfection complexes may also fuse with or alter sEV (Sato et al., 2016). Interestingly, over 50% of delivery vehicles, including lipid-based ones, which are endocytosed are released again from cells (Sahay et al., 2013; Sayers et al., 2019). Therefore, when late endosomes and lysosomes fuse with the plasma membrane to release sEV, transfection complexes could be re-released into the extracellular space alongside them and contaminate sEV preparations, even if cells have been extensively washed after transfection (Sahay et al., 2013; Sayers et al., 2019). This trafficking of transfection complexes is not surprising, as sEV can traffic similarly: sEV can be internalised into endosomes by one cell and released again to affect a second cell (Luga et al., 2012).

Here, we show that common transfection complexes have many physical properties which resemble sEV and that sEV preparations from transfected cells develop many physical signatures of these transfection complexes and are purified by standard sEV purification techniques. Furthermore, transfection of cells impairs the endogenous capacity of sEVs to deliver RNA to target cells. This suggests that transfection complexes alter and likely contaminate sEV preparations produced by cells. This could account

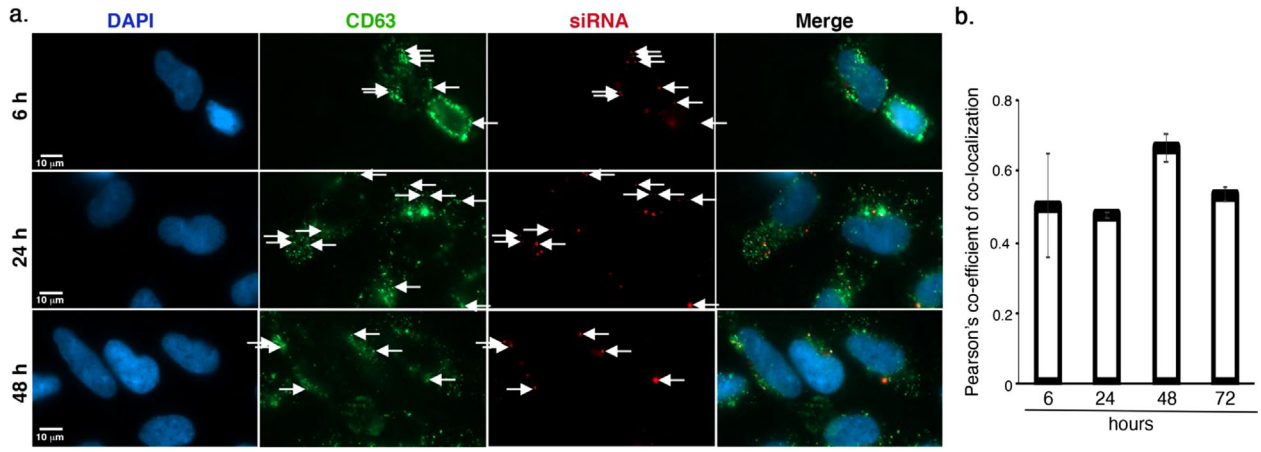

FIGURE 1 RNAiMax transfection complexes co-localize with late endosome and sEV markers. (a) Fluorescent microscopy of endogenous CD63 and siRNA transfected with RNAiMax in HEK293 cells 6, 24 and 48 h post-transfection. Arrows highlight siRNA colocalised with CD63. (b) Quantification of the colocalization of CD63 and siRNA delivered with RNAiMaX into HEK293 cells using the Pearson's correlation

for challenges in detecting delivery of RNA by sEVs in some experiments, and risks also causing artifacts where nucleic acid delivery by contaminating transfection complexes are attributed to sEVs.

2 | RESULTS

In transfected cells, much of the RNA persists in endosomes. To evaluate the amount of siRNA in the cytoplasm, and available for packaging into sEVs, we evaluated the siRNA dose eliciting maximal target knockdown as a surrogate for measuring the amount of siRNA in the cytoplasm. SiRNA targeting GFP was transfected into HEK293 cells stably expressing GFP using electroporation, the liposomal transfection reagent RNAiMax, and the cationic polymer transfection reagents INTERFERin and RiboJuice according to the manufacturer's instructions (Figure S1a-f). No sign of increased cell apoptosis or death was noted due to transfection (Figure S2). We also assessed multiple time points after transfection. Electroporation resulted in maximum target knockdown at 2 days post-transfection with a dose of 10 nM. For all other methods tested, differences in target knockdown were frequently not significant between concentrations; however, 5–10 nM siRNA concentration tended to cause maximal target knockdown, with higher significance for some reagents at 3 days (Figure S1a-f). For this reason, and because doses of siRNA higher than 10 nM can induce off-target effects (Caffrey et al., 2011), in subsequent experiments we selected an siRNA concentration of 10 nM.

To confirm previous literature that transfection complexes frequently colocalize with late endosomes and lysosomes (Liu et al., 2021; Sahay et al., 2013; Wittrup et al., 2015) where sEV are produced, fluorescent microscopy was used. To detect siRNA, a covalent 3′ fluorophore was used. CD63, a marker of the endolysosomal system, colocalised with a substantial proportion of siRNA transfected with RNAiMax, JetPrime or INTERFERin (Figure 1a,b, Figure S3). Co-localization of transfected siRNA was observed from 6 h to 48 h after transfection (Figure 1a,b). Although it is possible that the siRNA has separated from the transfection reagent in these results many previous studies demonstrate that a wide variety of lipid- and non-lipid-based transfection complexes colocalize with endosomes. And this pathway is so well-established that a major focus over the past 20 years on these reagents has aimed to engineer release of their cargoes from endosomes (Akinc & Battaglia, 2013; Gilleron et al., 2015; Hou et al., 2021; Hui et al., 1996; Kanasty et al., 2013; Kichler et al., 2001; Mok & Cullis, 1997; Selby et al., 2017; Wittrup et al., 2015; Zelphati & Szoka, 1996).

Transfection complexes localize to late endosomes with sEV and could be released to the extracellular space alongside sEV. The potential for transfection complexes to be mistaken for sEV and copurify with them was evaluated. Transfection complexes were prepared according to the manufacturer's instructions using GFP siRNA and the transfection reagents RNAiMax, INTERFERin and RiboJuice. In addition, we electroporated siRNA. The size of these transfection complexes and electroporated siRNA were compared using Nanoparticle Tracking (Figure 2a). No particles, or occasionally a much smaller number of particles were detected with media alone or siRNA alone. Polystyrene beads of 100 nm, and sEVs produced from two untransfected cell lines had average sizes of 100 and 100–150 nm, respectively, by Nanoparticle tracking (Figure 2a). Consistent with published results, electroporation of siRNA alone led to the appearance of particles in the same size range as exosomes (Figure 2a). These particles have been proposed to be precipitated RNA (Kooijmans et al., 2013). Particles of RNAiMAX, INTERFERin and RiboJuice transfection complexes had a median size (120–150 nm) closely resembling sEV (Figure 2a).

To test if transfection complexes could copurify with sEVs, transfection complexes were subjected to a standard ultracentrifugation protocol for sEV preparations. In these protocols, recovery of sEVs ranges from 10 to 75% (Lamparski et al., 2002; Muller

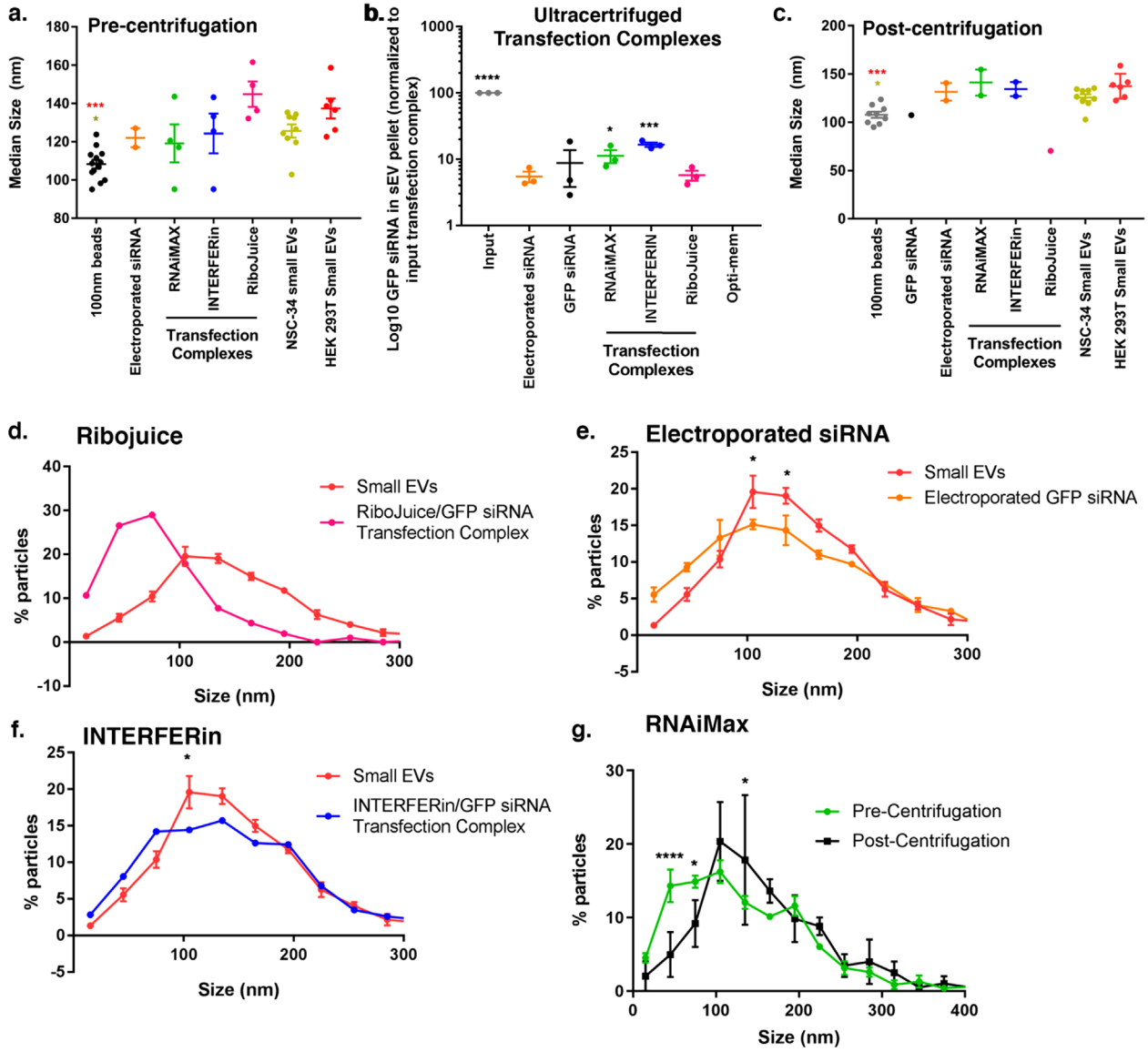

FIGURE 2 Transfection Complexes Have Similar Sizes as sEV and Pellet by Ultracentrifugation Using sEV Protocols.(a) Median sizes of sEV from HEK293 cells and the indicated transfection complexes in solution without any centrifugation as obtained by Nanoparticle tracking analysis. One-way ANOVA Tukey's multiple comparisons test. (b) Amount of input siRNA in transfection complexes recovered by ultracentrifugation using a standard sEV protocol on a Log10 scale. RT-qPCR for siRNA targeting GFP after ultracentrifugation and recovery of transfection complexes using standard sEV protocols. (c) Median sizes of sEV from HEK293 cells and the indicated transfection complexes recovered by ultracentrifugation using Nanoparticle tracking analysis. Note, measurable particles were only detected in one experiment with RiboJuice and GFP siRNA in these conditions. (d-f) Size profile of sEV from HEK293 cells vs. transfection complexes (precentrifugation) for (d) RiboJuice (e) Electroporated siRNA and (f) INTERFERin measured using Nanoparticle tracking analysis. Two-way ANOVA Dunnett's multiple comparisons test in relation to HEK 293T sEVs. (g) Size profile measured using Nanoparticle tracking analysis of RNAiMax transfection complexes before and after ultracentrifugation using a standard sEV protocol. In d-f size profiles of sEV and transfection complexes were performed in independent preparations (electroporated siRNA, INTERFERin, RNAiMax n = 2, RiboJuice n = 1) and average size +/- standard error is shown. * $p < 0.05$, *** $p < 0.001$ ANOVA

et al., 2014). Similarly, quantification by RT-qPCR of RNA in pellets of transfection complexes compared to that in transfection complex inputs showed that 10–20% of GFP siRNA in RNAiMax, INTERFERin and RiboJuice transfection complexes was recovered in the pellet after ultracentrifugation using the sEV protocol (Figure 2b). The median size of transfection complexes recovered after ultracentrifugation was again similar to sEV (Figure 2c). In some circumstances particles were only detected in one or two of the three ultracentrifuged preparations examined (Figure 2c, RiboJuice, GFP siRNA). At the same time, siRNA in these complexes was consistently detected by RT-qPCR (Figure 2b). This is likely because the number of transfection complexes required to transfect cells is low, and with the loss due to ultracentrifugation, the particle number falls below the background level of the nanoparticle tracking system while the siRNA remains quantifiable by RT-qPCR.

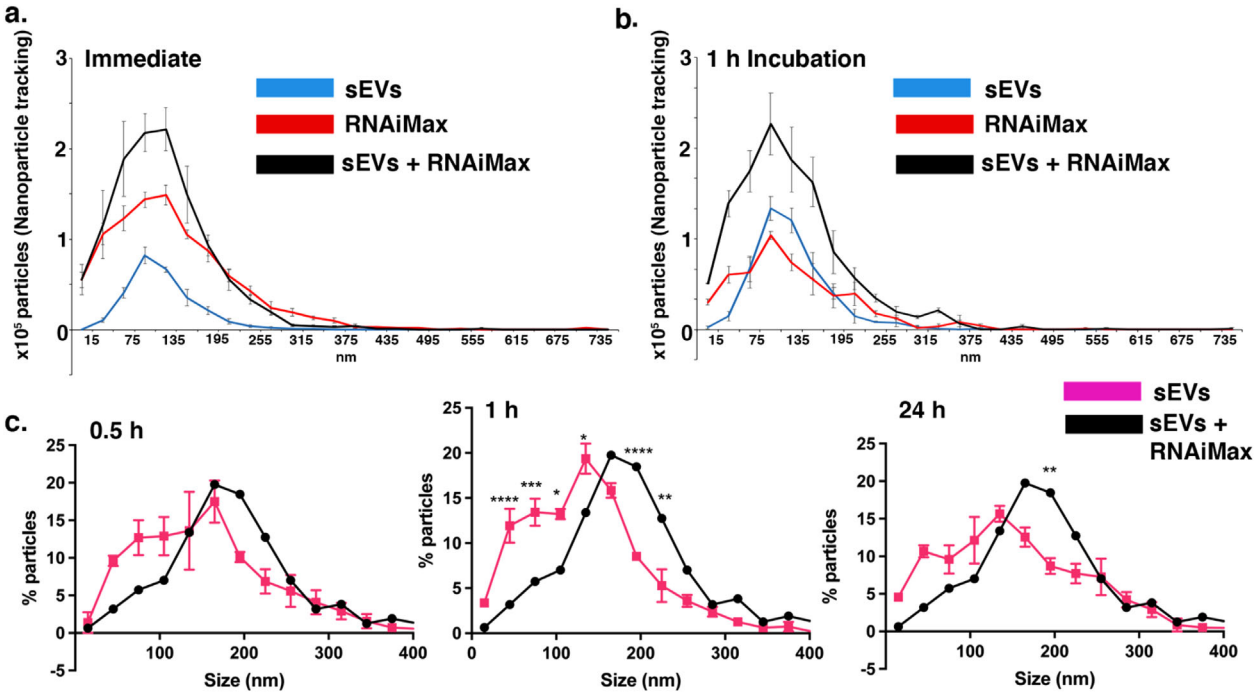

FIGURE 3 Transfection complexes and sEV do not exhibit significant formation of hybrids (a,b) sEVs from HEK293 cells and RNAiMax transfection complexes were mixed and their numbers were tested immediately (a) and after 1 h incubation using Nanoparticle tracking analysis. (b). (c) Size profile of sEVs from HEK293 cells and sEVs mixed with RNAiMax transfection complexes after 0.5, 1 and 24 h as analysed by Nanoparticle tracking analysis. Size profiles of sEV and transfection complexes were performed in at least three independent preparations and average size +/- standard error is shown. * $p < 0.05$, ** $p < 0.01$, *** $p < 0.001$ ANOVA

A more detailed analysis of the size profile of RiboJuice complexes showed that they were frequently smaller than sEV (Figure 2d). Ultracentrifugation of electroporated siRNA generated a size profile of particles similar to sEV (Figure 2e). After ultracentrifugation, RNAiMax and INTERFERin transfection complexes tended to have a higher median size and a broader range of sizes than sEV (Figure 2f, g, Figure S4). Notably, after ultracentrifugation the size of RNAiMax transfection complexes was larger (Figure 2g). This could be caused by pelleting of larger transfection complexes, or other phenomena like aggregation or fusion of transfection complexes induced by elevated forces during ultracentrifugation. Therefore, if transfection complexes are released by cells, they will copurify with sEV using standard protocols and exhibit sizes closely resembling sEVs using Nanoparticle Tracking.

If transfection complexes are present in late endosomes with sEV they may fuse with them or remain separate and be released alongside them. To test whether transfection complexes can fuse in substantial numbers with sEV we analysed both separately and after coincubation in the absence of cells. Co-incubation of sEV and RNAiMax transfection complexes resulted in a number of particles equal to the sum of sEV and transfection complexes (Figure 3a,b). This demonstrates that very few, if any sEV fused with RNAiMax transfection complexes when incubated for up to an hour. After coincubation of sEV and RNAiMax transfection complexes for up to 24 h, the size distribution of particles was broadened representing an average of sEV and transfection complexes (Figure 3c, Figure S4). These incubations were also performed at the pH of early and late endosomes (pH 6.5 and 5.5) where sEV and transfection complexes likely encounter one another. Mixing RNAiMax complexes and sEV resulted in particles of intermediate size between these two, and no size change in particles was observed after incubation of RNAiMax complexes and sEVs (Figure S5). This suggests that sEV and RNAiMax transfection complexes do not fuse, or fuse in very small proportions, but that transfection complexes would be released alongside sEV and contaminate sEV pellets from transfected cells.

To test for signs that RNAiMax transfection complexes contaminate sEV preparations, extracellular particles were prepared from media of transfected cells using the standard sEV ultracentrifugation protocol. Equal numbers of particles from sEV preparations from transfected and untreated cells were analysed by Western blot for sEV markers including Alix and Flotillin2 (Figure 4a). The average number of miRNAs per particle in sEVs including miR-15b and miR-106a also were also measured by RT-qPCR (Figure 4b). Neither levels of sEV protein markers or RNAs were decreased substantially by transfection. The number of particles purified by ultracentrifugation from transfected cells was slightly increased compared to untransfected cells (Figure 4c). Together, this argues that RNAiMax transfection complexes may be present in sEV preparations but do not substantially dilute the amount of sEVs or account for a major proportion of ultracentrifuged particles.

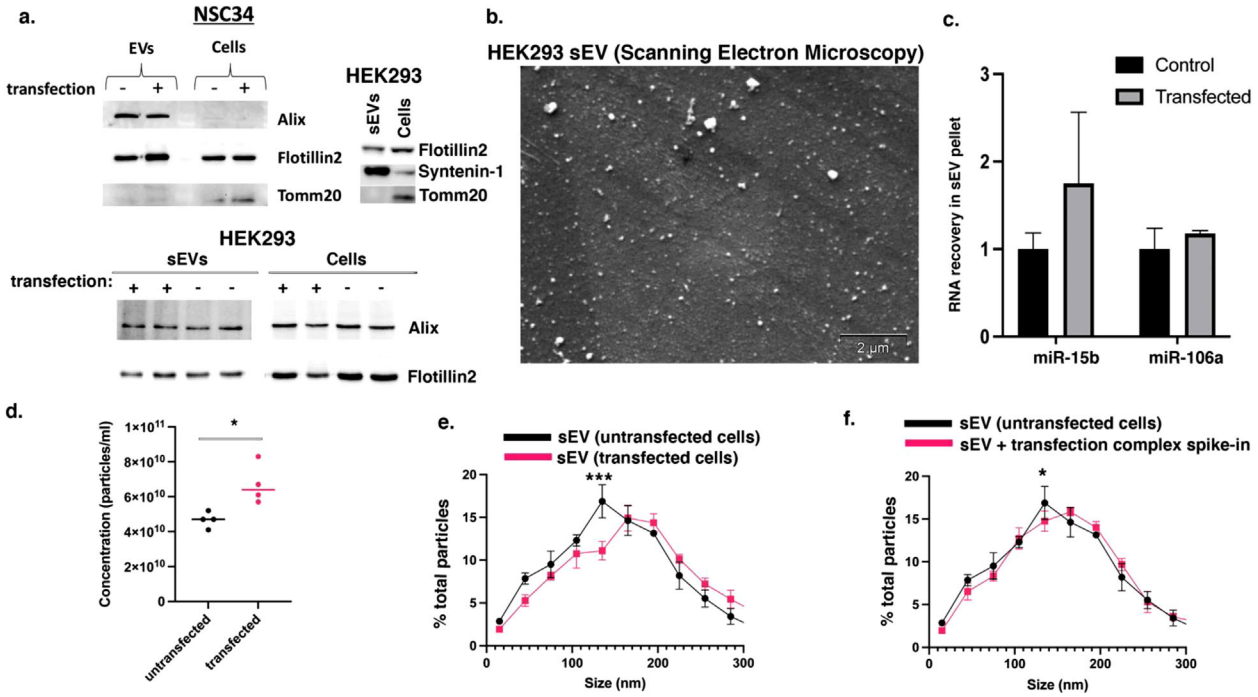

FIGURE 4 Transfection Complexes Comprise a Small Proportion of Particles Retrieved by Ultracentrifugation of Media From Transfected Cells. (a) Western blot for sEV markers in sEV preparations from NSC-34 or HEK293 cells transfected or not 3 days ago with RNAiMax. Equal numbers of particles were loaded in each lane for sEV preparations. (b) RT-qPCR for miRNAs in sEV preparations from HEK293 cells transfected or not 3 days ago with RNAiMax. Equal numbers of particles were used for each RNA preparation from sEV preparations. (c) Number of particles per ml obtained in sEV preparations from HEK293 cells transfected or not 3 days ago with RNAiMax. (d) Size profile of sEV preparations from HEK293 cells transfected or not 3 days ago with RNAiMax. Note the shift to larger particle size in sEV preparations from transfected cells. Two-way ANOVA Sidak's multiple comparisons test (e,f) Potential for transfection complexes to cause a shift in the size profile of sEV preparations. (e) Relative particle number of sEV from HEK293 cells and RNAiMax transfection complexes mixed together in (f) and measured using Nanoparticle tracking analysis. (f) Size profile of sEVs from untransfected HEK293 cells vs. sEV spiked with approximately 2% the relative number of RNAiMax transfection complexes measured using Nanoparticle tracking analysis. Note the slight shift to larger sizes of particles induced by the transfection complex spike-in that resembles the size shift of sEV preparations from transfected cells in (d). Two-way ANOVA Dunnett's multiple comparisons test

Transfection complexes of RNAiMax purified by ultracentrifugation exhibited larger sizes (Figure 2g). By Nanoparticle tracking analysis, sEV preparations from cells transfected with RNAiMax had a broader size distribution, including a significant shift toward larger particle sizes compared to preparations from untransfected cells (Figure 4d, Figure S4). This size shift resembles the size profile of ultracentrifuged RNAiMax transfection complexes (Figure 2g). To determine if this could be due to contaminating transfection complexes, we spiked ultracentrifuged RNAiMax transfection complexes into sEV preparations, at a ratio of about one transfection complex per 50 sEVs (Figure 4e). This ratio was selected because data above suggests that the number of contaminating RNAiMax transfection complexes is probably much lower than the number of sEVs. This caused a slight shift toward larger particles (Figure 4f) resembling that of sEV preparations from transfected cells (Figure 4d). This suggests that contaminating transfection complexes represent a small percentage of particles in sEV preparations of transfected cells. As transfection complexes contain large amounts of siRNA per particle, this small percentage of RNAiMax transfection complexes could account for a large proportion of transfected RNA in sEV preparations.

To evaluate in more detail if transfection complexes may contaminate sEV preparations from transfected cells we performed a lipidomic analysis of RNAiMax transfection complexes, sEV, and sEV from cells transfected with RNAiMax. A Partial Least Squares-Discriminant Analysis (PLS-DA) of the lipid profile of these samples demonstrated a complete separation of sEVs from transfected and untransfected cells (Figure 5a), indicating that transfection with RNAiMAX is affecting the lipidome of sEVs preparations (Figure 5a). Several lipids were over-represented in RNAiMax transfection complexes by 10–1000-fold. These lipids tended to be modestly enriched in sEVs preparations from transfected cells compared to the lipid profile of untransfected cells (Figure 5b). This provides evidence that lipids from transfection complexes are present in sEV preparations from transfected cells. These lipids could have integrated into cell membranes and subsequently been included in sEVs during their budding from cell membranes. Alternatively, these lipids could be in sEV preparations due to the presence of contaminating transfection complexes. To help differentiate these two possibilities we utilised Optiprep density gradients. On Optiprep density gradients of RNAiMax transfection complexes, the siRNA floated to the top of gradients (fraction 1–2, density < 1.05, Figure 5c,d). When sEV pellets from transfected cells were analysed on identical Optiprep gradients, protein markers of sEVs were detected as expected

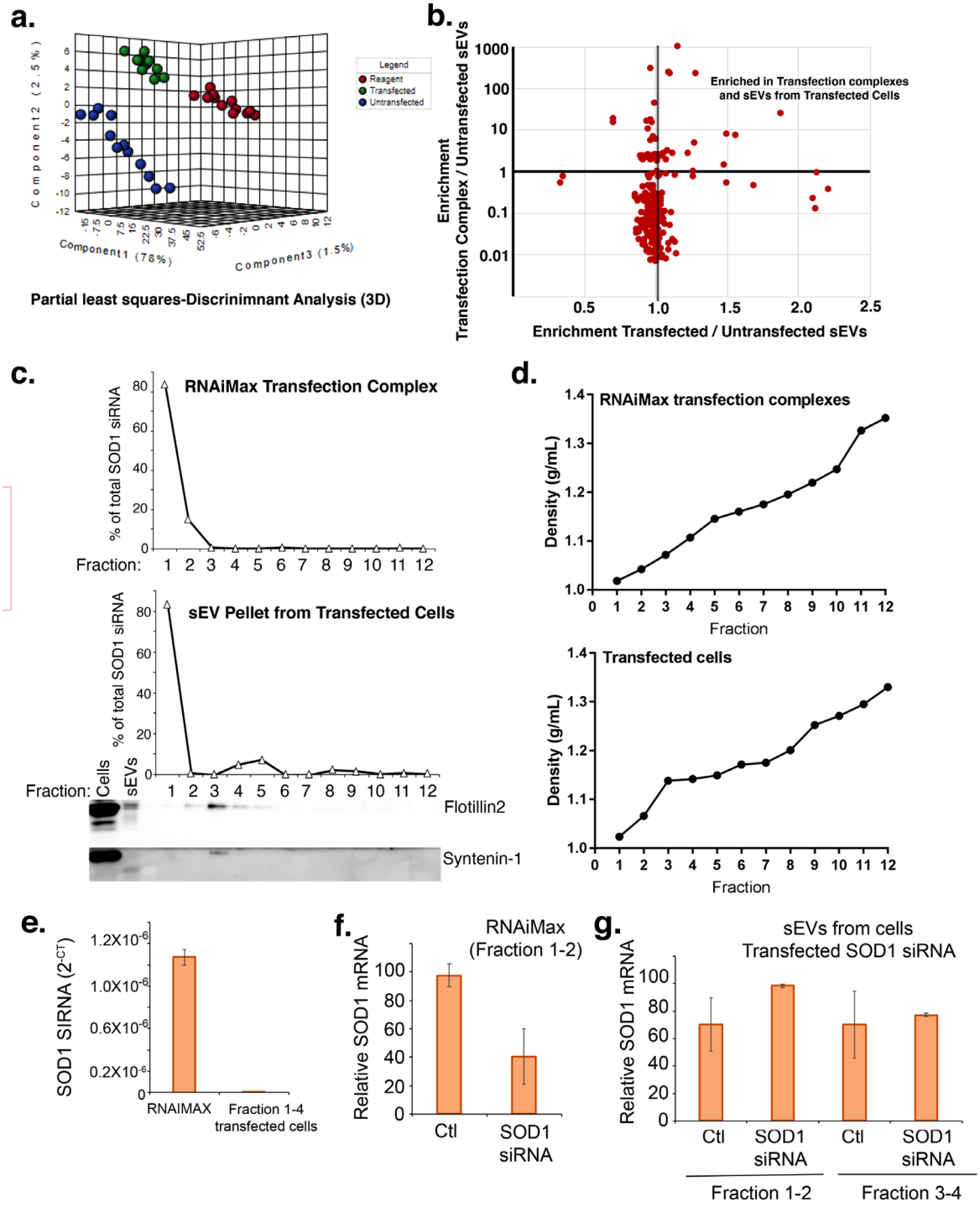

FIGURE 5 Evidence of RNAiMax transfection complexes contaminating sEV pellets from transfected cells. (a) 3-D Partial Least Squares–Discriminant Analysis (PLS-DA) of the lipidome of RNAiMax transfection complexes (Reagent), sEVs, and sEVs from transfected cells. (3 components; 10-fold cross validation $R^2 = 0.9982$ and $Q^2 = 0.9975$; p-value < 0.001 for 1000 permutations). (b) Plot of the enrichment of lipids in RNAiMax transfection complexes / untransfected sEVs (y-axis) vs. lipids enriched in sEVs from transfected / untransfected cells. Lipids in the upper right quadrant are both enriched in RNAiMax transfection complexes and sEV pellets from transfected cells compared to sEVs from untransfected cells. (c,d) Optiprep gradient analysis of RNAiMax transfection complexes and sEVs pellets from transfected cells. sEVs are enriched in fractions 2–5 as indicated by Western blot for sEV markers (Flotillin2, Syntenin-1) and sEV characteristic density of 1.05–1.2 (d) RT-qPCR for SOD1 siRNA in RNAiMax transfection complexes indicates that this is predominantly found in fraction 1 in both pure RNAiMax transfection complexes and sEV pellets from cells transfected with RNAiMax. (e) Quantification by RT-qPCR of siRNA targeting *SOD1* in RNAiMax transfection complexes freshly prepared, or in fractions enriched in RNAiMax transfection complexes from sEV preparations from transfected cells. (f) Quantification by RT-qPCR of *SOD1* mRNA after incubation of HEK293 cells with RNAiMax transfection complexes isolated by iodixanol density gradient compared to controls treated with PBS (g) Quantification by RT-qPCR of *SOD1* mRNA after incubation of HEK293 cells with fractions 1–2, or fractions 3–4 from iodixanol gradients of sEV preparations from cells transfected with RNAiMax complexes containing SOD1 siRNA or a control siRNA

at distinct densities of 1.05–1.15 in fraction 3–5 (Figure 5c,d). The siRNA transfected into these cells with RNAiMax prior to collection of sEVs was most abundant at a density < 1.05, like RNAiMax transfection complexes, although a small amount of this siRNA was also detected in fractions containing sEVs (Figure 5c). Together, this suggest that RNAiMax transfection complexes detected by their size, lipid profile and distinct density contaminate sEV preparations from transfected cells (Figures 4 and 5).

With the aim of testing whether transfection complexes contaminating sEV preparations could deliver siRNA, we fractionated sEV pellets from cells transfected with siRNA recognizing SOD1 on density gradients. In parallel we subjected freshly prepared transfection complexes containing the same siRNA targeting SOD1 to density gradients. Fractions of sEV pellets from transfected cells contained 10,000-fold less siRNA than the input RNAiMax transfection complexes recovered on density gradients (Figure 5e). RNAiMax complexes purified on density gradients could reduce expression of *SOD1* mRNA by a moderate 60% in target cells (Figure 5f). sEVs packaged with SOD1 siRNA by stably expressing it in the pre-miR-451 backbone could also reduce *SOD1* mRNA levels in target cells (Figure S6). In contrast, density gradient fractions of sEV pellets from transfected cells could not (Figure 5g). The lack of effect observed with contaminating transfection complexes in these sEV pellets may be due to the poor recovery of contaminating transfection complexes due to the impact of iodixanol on transfection complexes, as pH, osmolarity and buffer composition all impact the stability, and activity of transfection complexes and related delivery vehicles. This latter possibility seems likely, as RNAiMax transfection complex particles purified on iodixanol gradients had only a modest ability to reduce target mRNA expression, even when these were added at a particle number 10-20-fold higher than freshly prepared transfection complexes (20,000 particles per cell vs. 1000 particles per cell).

To overcome these limitations we pursued this analysis omitting the density gradient fractionation. Whether siRNAs were transfected using electroporation, RNAiMax, INTERFERin or RiboJuice only between 0.01% and 0.001% of siRNA transfected into cells was recovered in ultracentrifuged sEV preparations (Figure 6a). Transfection complexes contain very large amounts of siRNA per particle. For example, lipid-based reagents are usually formed at ratios of amine (lipid): phosphate (nucleic acid) of 1:2 to 1:10 with an encapsulation efficiency of over 80% (e.g., Love et al., 2010). This means that even if a small proportion of transfection complexes contaminate sEV preparations, they can account for an outsized proportion of the RNA in sEV preparations. sEV pellets from cells transfected with RNAiMax contained on average 0.1 copy of siRNA per particle while those from cells with other transfection methods generally contained less siRNA (Figure 6b). This is similar to or slightly lower than the abundance of siRNA in sEV when these were stably expressed from the pre-miR-451 backbone (Reshke et al., 2020), or the level of the most abundant miRNA in sEV (Chevillet et al., 2014).

We recently published that sEV produced by cells stably expressing siRNA incorporated in the pre-miR-451 backbone is more efficient at delivering siRNA into target cells and reducing expression of mRNA targets than lipid nanoparticles (Reshke et al., 2020). Therefore, if siRNA in sEV preparations is in contaminating transfection complexes these sEV preparations should have diminished capacity to deliver siRNA to target cells. The number of sEVs added to recipient cells was normalised to their content of SOD1 siRNA. Knockdown of *SOD1* mRNA was observed with sEVs packaged using stable expression at approximately 10-fold lower doses than sEVs prepared from cells transfected with the same siRNA using RNAiMax (Figure 6c). Together (Figures 4–6), this suggests that siRNA in sEV preparations from transfected cells is contained in contaminating transfection complexes and this causes these sEV preparations to be less efficient at siRNA delivery than sEVs from untransfected cells.

It is also possible that when transfection complexes accumulate in, fuse with and damage endosomes that sEVs formed from and harboured within these organelles are altered along with their capacity to deliver RNA cargoes. To test this, cells stably expressing siRNAs targeting alpha-synuclein in the pre-miR-451 backbone were left untreated or transiently transfected with a control siRNA using RiboJuice, INTERFERin or RNAiMAX. sEV preparations from these cells were incubated with recipient SH-SY5Y cells which endogenously express alpha-synuclein. Knockdown of alpha-synuclein mRNA in SH-SY5Y cells of approximately > 70% was observed with sEVs produced by untreated cells compared to sEVs transfected with control GFP siRNA or no siRNA (Figure 6d-f). In contrast, sEV preparations from cells transfected with a control siRNA (Figure 6d-f) using any of the transfection reagents (RNAiMax, INTERFERin, RiboJuice) showed little or no target knockdown in recipient cells (Figure 6d-f). Similarly, transfection of cells with a nonsilencing siRNA using RNAiMax also prevented the sEVs produced by these cells from delivering GFP siRNA and decreasing GFP fluorescence measured by flow cytometry (Figure 6g) As the packaging into sEVs of siRNA integrated into the pre-miR-451 backbone is independent of Ago2[14], this effect cannot be accounted for by competition for miRNA machinery. Confirming this, the levels of siRNA targeting GFP and alpha-synuclein in sEVs were not significantly altered by transfection with RNAiMax (Figure 6h). In a dose-response, it took at least 10-fold more sEVs from cells transfected with RNAiMax to knockdown alpha-synuclein, than sEVs from untransfected cells (Figure 6i). These effects suggest that endosome functions are disrupted by transfection, and this alters sEVs produced by these cells in a manner which reduces their ability to deliver their siRNA cargoes.

Cumulatively, these results suggest that transfection complexes accumulate in late endosomes where sEV are formed and contaminate sEV preparations produced from these cells. This creates a risk of nucleic acid delivery by contaminating transfection complexes being wrongly ascribed to sEVs. Transfection also alters the sEV produced by cells in a way that disrupts their endogenous capacity to deliver RNA cargoes into target cells. This risks obscuring the endogenous capacity of sEVs to deliver their cargoes.

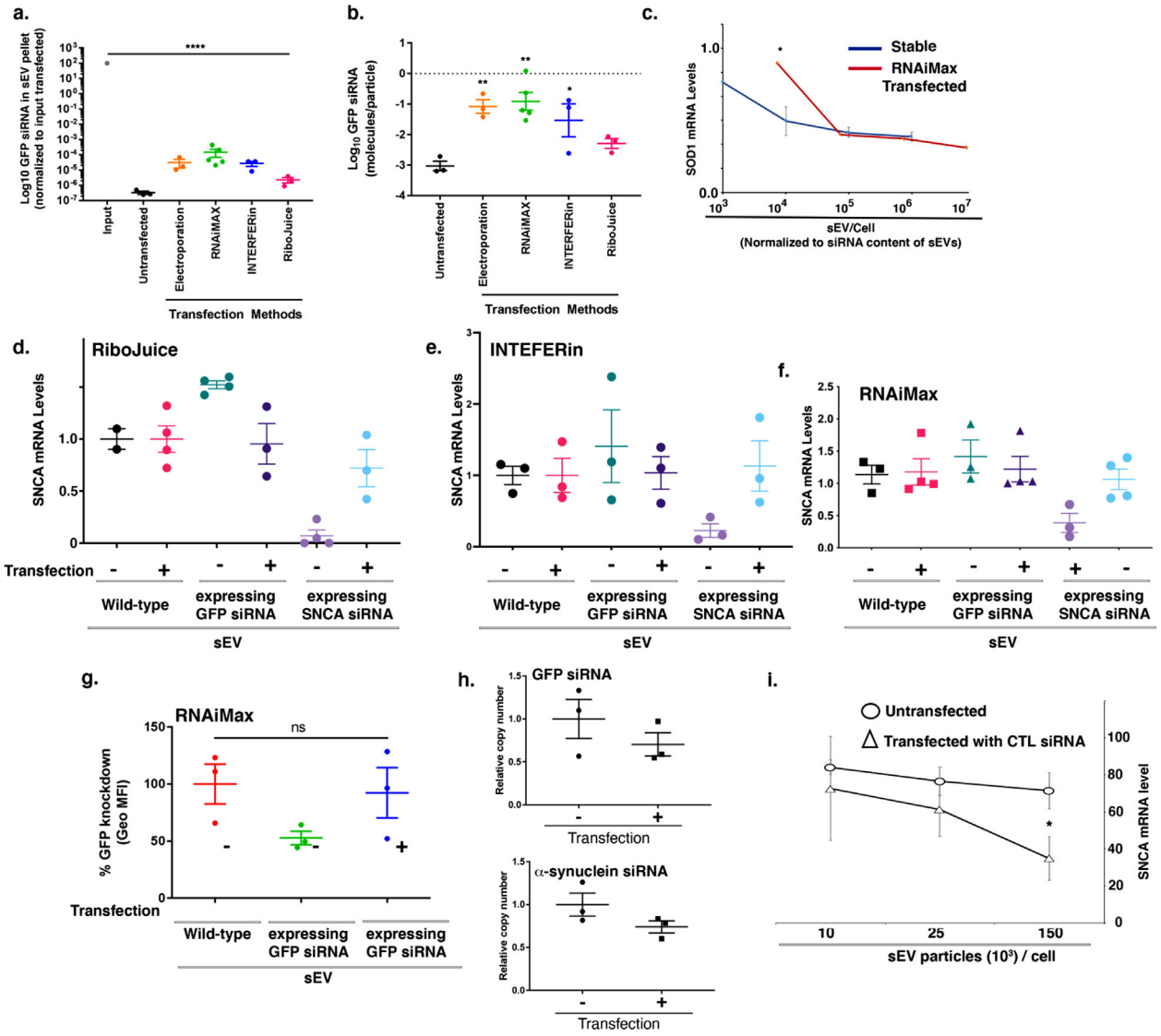

FIGURE 6 Transfection Impairs the Ability of Endogenous Extracellular Vesicles to Deliver RNA Cargoes.(a) RT-qPCR quantification on a Log10 scale of siRNA targeting GFP in sEV preparations from HEK293 cells 3 days after transfection of cells by the indicated methods. (b) Quantification of siRNA targeting GFP by RT-qPCR per particle in sEV preparations 3 days after transfection of HEK293 cells by the indicated methods. (c) Quantification of SOD1 mRNA by RT-qPCR in mixed motor neurons after treatment with various doses of sEVs packaged with siRNA targeting SOD1 by stable expression from the pre-miR-451 backbone (stable) or by transfection using RNAiMax. sEV doses were normalised to relative SOD1 siRNA quantity. (d-f) Quantification of *SNCA* mRNA by RT-qPCR 3 days after treatment of SH-SY5Y cells with sEVs prepared from wild-type HEK293 cells or HEK293 cells stably expressing either siRNA targeting GFP (control), or *SNCA*. sEV-producing cells were transfected or not with control nonsilencing siRNA using (d) RiboJuice (e) INTERFERin or (f) RNAiMax 3 days prior to collection of sEVs. (g) Quantification of GFP protein fluorescence by flow cytometry 3 days after treatment of human fibroblasts stably expressing GFP with sEVs prepared from wild-type HEK293 cells or HEK293 cells stably expressing siRNA targeting GFP. sEV-producing cells were transfected or not (+/-) with control nonsilencing siRNA using RNAiMax 3 days prior to collection of sEVs. (h) Quantification by miSCRIPT RT-qPCR of siRNA targeting GFP or alpha-synuclein in sEVs from HEK293 cells stably expressing these siRNA from the pre-mIR-451 backbone. HEK293 cells were previously transfected, or not (+/-), with RNAiMax. (i) Quantification of alpha-synuclein mRNA after incubation of SH-SY5Y cells with sEV packaged with siRNA targeting alpha-synuclein by stable expression from the pre-miR-451 backbone at the indicated doses. Statistics: One-way ANOVA Dunnett's multiple comparisons test in relation to treatment with WT HEK 293T sEVs

3 | DISCUSSION

Transfection is a simple, rapid way to introduce nucleic acids into cells. Transfection complexes, however, have non-negligible effects on cells, particularly on the endolysosomal system where they accumulate, persist and disrupt endosomes (Du Rietz et al., 2020; Gilleron et al., 2013; Gilleron et al., 2015; Kanasty et al., 2013; Wittrup et al., 2015). Previous studies have noted that between 50% and 80% of all lipid-based delivery vehicles internalised by cells are exocytosed into the extracellular space (Sahay et al., 2013; Sayers et al., 2019). Similarly, nanoparticles of many different materials are internalised by cells, accumulate in late

endosomes, and are exocytosed in large numbers by cells (Behzadi et al., 2017). Transfection complexes resemble lipid nanoparticles in their composition and trafficking. These studies raise the possibility that transfection complexes or lipid nanoparticles will be exocytosed alongside sEVs and contaminate preparations of sEVs.

Transfection complexes based on lipids, polymers or receptor ligands evidently vary in their physical properties, but they usually exhibit properties that would allow them to copurify with and be mistaken for sEVs. Many others have previously shown that lipid-based transfection complexes similar to those used here, have a size distribution of 50–200 nm, like sEVs (Kim et al., 2021; Kulkarni et al., 2018; Ogris et al., 1998; Sork et al., 2016; Whitehead et al., 2014), as we observed. Interestingly, transfection complexes often exhibit densities of 1.05–1.20 g/ml resembling sEVs as well (Sork et al., 2016; Wheeler et al., 1999). By electron microscopy lipid-based nanoparticles and transfection complexes also closely resemble sEVs in size and appearance (Kulkarni et al., 2018; Ogris et al., 1998; Whitehead et al., 2014), frequently even exhibiting a cup-like appearance considered a defining characteristic of fixed sEVs. Lipid nanoparticles are often purified by tangential flow filtration and can also be pelleted by ultracentrifugation, like sEVs (Mihaila et al., 2011). Together with the findings presented above, this suggests that approximately 50–70% of transfection complexes applied to cells will be released again by cells after internalization, and will contaminate sEV preparations and mimic sEVs using many of the standard techniques used in sEV characterization. The challenge of detecting contaminating transfection complexes in sEV preparations would be even more acute if the percentage of transfection complexes per sEV is low, as our results suggest (Figures 4 and 5). Because transfection complexes contain orders of magnitude more of a specific nucleic acid (e.g., 100′s to 1000′s per particle) compared to sEVs, this small percentage of contaminating transfection complexes can account for a very large proportion of the nucleic acid in sEV preparations from transfected cells (e.g., Figure 5). This means that when cells are transfected, there is a substantial risk that any intercellular transfer observed with sEV preparations is due to contaminating transfection complexes.

Other studies have aimed to use transfection complexes to introduce nucleic acids into sEVs (Busatto et al., 2021; Evers et al., 2021; Piffoux et al., 2018; Shtam et al., 2013). Our results suggest there is a distinct risk in doing this that transfection complexes would subsequently purify with sEVs and this could be mistakenly construed as sEVs being transfected.

Transfection of cells has been frequently used to demonstrate that sEVs can deliver nucleic acids into the cytoplasm of target cells (e.g., Kojima et al., 2018; Ohno et al., 2012; Ridder et al., 2015; Wang et al., 2018). Transfection with lipid nanoparticles has also been proposed as a way to load sEVs with nucleic acids (Maugeri et al., 2019). If, transfection complexes contaminate sEV preparations, or are retained by cells and exocytosed in large quantities with sEVs, then the cited examples and many more in the literature could be due to contaminating transfection complexes. There may be methods which allow the separation of some formulations of some transfection complexes and sEVs in some circumstances, as demonstrated by Figure 5 and the accompanying manuscript from McConnell *et al.* A more robust solution is to consistently use stable expression systems to study sEV delivery to target cells. Even in this, caution may be required. Lentiviral particles, for example, also exhibit many physical characteristics of sEVs and it is possible that sEV preparations from cells recently incubated with lentiviral particles could be contaminated with lentivirus.

The results of McConnell *et al.* demonstrate that some types of transfection complexes contaminate sEV preparations, and these contaminating transfection complexes retain their activity after separation on density gradients. In our experiments, RNAiMax transfection complexes which contaminate sEV preparations had minimal or no capacity to deliver siRNA after iodixanol gradients (Figure 5). Nonetheless, when this density gradient centrifugation step was omitted, RNAiMax transfection complexes which contaminate sEV preparations retained the capacity to deliver siRNA (Figure 6). This difference between the results of McConnell *et al.* and those presented here could be due to differences in the types of transfection complexes and density gradient protocols used.

It is important to note that in this study we have used a small selection of the wide array of transfection reagents and delivery vehicles in use. The present results cannot be assumed to apply to all of these, or even the ones used here if prepared in alternative manners. Nonetheless, with other literature defining the characteristics of transfection reagents and delivery vehicles, the data presented here should provide a cautionary message for many studies employing transfection reagents to study extracellular vesicles. It is possible that reagents used to introduce proteins into cells could be subject to similar complications.

In studies of sEVs the relative dose of silencing RNAs, miRNAs or mRNAs required to observe an effect in target cells is not frequently determined. Where it has been, the dose of nucleic acid required to mediate effects when delivered by sEV is frequently similar to or exceeds that required by lipid nanoparticles or transfection complexes (Alvarez-Erviti et al., 2011; Didiot et al., 2016), which only deliver 0.1% or less of their cargoes into the cytoplasm (Gilleron et al., 2013; Pei et al., 2010). We recently published that sEVs packaged with siRNA from a stably expressed vector are 30-fold or more efficient at RNA delivery than a lipid nanoparticle (Reshke et al., 2020). Subsequent studies have similarly shown that sEVs packaged with a stably expressed RNA are more efficient delivery vehicles than lipid nanoparticles and several transfection reagents (Murphy et al., 2021). We estimated that sEVs deliver between 10 and 100% of their cargoes into the cytoplasm. Other recent studies using split reporter systems suggest that approximately 25% of sEVs deliver their cargoes into the cytoplasm of target cells (Joshi et al., 2020). In studies of sEVs where the observed nucleic acid delivery may be due to contaminating transfection complexes, one might expect the delivery efficiency to be much reduced and similar to that of transfection complexes.

Transfection complexes and lipid nanoparticles accumulate in late endosomes where sEVs are produced and where they concentrate after being internalised by cells (Hou et al., 2021; Piotrowski-Daspit et al., 2020; Rehman et al., 2013; Wittrup et al., 2015). Impacts of transfection complexes on endolysosomal trafficking have previously been described, raising cautions about using transient transfection to study the endolysosomal system (Jonker et al., 2017). The data presented here suggests that cells transfected with several common transfection reagents produce sEVs that have lost most of their capacity to deliver their RNA cargoes. Several mechanisms could underlie these effects. It is possible that transfection complexes directly contact and alter sEVs, but they could also alter sEV production by altering the pH of late endosomes by absorbing protons, by fusing with endosomal membranes or inducing endosomal damage and recruitment of membrane repair processes (Jonker et al., 2017; Kanasty et al., 2012; Liu et al., 2021; Van De Vyver et al., 2020; Wittrup et al., 2015). This suggests that the use of transient transfection may also obscure the physiological effects of sEVs. Given the important amounts of transfection reagents and delivery vehicles which persist in the endolysosomal system (Dowdy, 2017; Gilleron et al., 2013; Hou et al., 2021; Rehman et al., 2013; Selby et al., 2017; Wittrup et al., 2015), one would also expect that transfection of recipient cells would risk altering sEV uptake and fusion through endocytic pathways.

The results presented here provide a cautionary note on the use of transient transfection to study sEVs, and strongly recommend the use of stable expression systems for studies of sEV production and delivery, and for their use as therapeutic delivery vehicles.

4 | MATERIALS AND METHODS

4.1 | Cell lines

NSC-34 (Cedarlane), HEK 293T (ATCC) and SH-SY5Y (ATCC) cells were used in this study. SH-SY5Y cells were differentiated with retinoic acid prior to incubation with sEV. HEK 239A with GFP knocked-into the AAVS1 locus using CRISPR was obtained from Ryan Russell (University of Ottawa). emGFP was knocked-in with CRISPR technology. HEK 293T expressing GFP siRNA in a pre-miR-451 backbone was previously described (Reshke et al., 2020). Neonatal normal human dermal fibroblast (NHDF-Neo) (Cedarlane, CC-2509) were transduced with lentivirus (pLVX-AcGFP1-N1 vector, Clontech, 632154)

4.2 | Cell culture

Cells were cultured in DMEM (Wisent Bioproducts, 319-015-CL) supplemented with 10% heat inactivated FBS (Wisent Bioproducts, 081–150) and 1% Penicillin–Streptomycin (Wisent Bioproducts, 450-201-EL). Cells were cultured at 37°C 5% CO_2 in humidified incubators. Cells were washed with 1X PBS (pH 7.4, without calcium and magnesium) (Wisent, 311-010-CL) and then dissociated using Trypsin/EDTA (0.25%/EDTA 2.21 mM in HBSS) (Wisent Bioproducts, 325-043-EL). The trypsin was neutralised with at least one equal volume of culture media. The concentration of cell suspensions was determined using a hemacytometer (Sigma, Z359629 or Thermo Fisher Scientific, 0267110).

Human SH-SY5Y neuroblastoma cells were plated in a 24-well plate at a density of 5×10^4 cells per well (~50% confluence) in complete media: DMEM (Wisent Bioproducts, 081–150) supplemented with heat inactivated 10% FBS (Wisent Bioproducts, 081–150) and 1% penicillin-streptomycin (Wisent Bioproducts, 450-201-EL). After 24 h, differentiation was induced by lowering the FBS in culture media to 1% without antibiotics and adding 10 μM all transretinoic acid (RA) (Sigma-Aldrich Cat.no. R2625) at day 1, 4, and 7. At day 8 the differentiated cells were treated with 50,000 sEVs per cell, calculating the dose using Nanoparticle tracking. Then, after 72 h of incubation with sEVs, the cells were treated with TRIzol reagent for RNA isolation.

4.3 | siRNAs

siRNAs targeting SOD1 and GFP siRNA were annealed from single strands custom-synthesised by IDT. SOD1 siRNA (UUCAGUCAGUCCUUUAAUGCUU) and complementary strand (GCAUUAAAGGACUGACUGAA) or GFP siRNA (AUGAACUUCAGGGUCAGCUUGC) and complementary strand (AAGCUGACCCUGAAGUUCAUU) were annealed at a 10μM concentration in 10X T4 DNA Ligase Reaction Buffer (NEB, B0202S) with a final reaction volume of 100μl during a 10 min incubation at 95°C, with a gradual cool down of 0.1°C/sec to 25°C for 1 min. Control siRNA was Silencer select negative Control No.2 siRNA (Thermo Fisher Scientific, 4390846). Fluorescent siRNA was siGLO Cyclophilin B Control siRNA fluorescently labelled with DY-547 (Human/Mouse/Rat) (Dharmacon, D-001610-01-05).

4.4 | Ultracentrifugation protocol for preparation of sEV and analysis of transfection complexes

Cells were grown to 70–80% confluence. DMEM was removed, followed by a 1X PBS wash, to remove any remnants of contaminating small EVs originating from the FBS in the DMEM, then replaced with UltraCULTURE serum-free medium for three days. UltraCULTURE conditioned media collected from cells was centrifuged at 300x g maximum (TX-400 rotor, k-factor 143450 Thermo Fisher Scientific) for 10 min, at 2000x g maximum (TX-400 rotor, Thermo Fisher Scientific) for 10 min and again at 10,000x g average (F15-6x-100y rotor, k-factor 1490, Thermo Fisher Scientific) for 30 min. The supernatant was then centrifuged at 100,000x g average (SW 40 Ti, SW 41 Ti or SW 32 Ti Swinging-Bucket rotors; rotor k-factors 277, 256, 256, respectively, Beckman Coulter Life Sciences) in thick wall polycarbonate tubes (Beckman Coulter Life Sciences, 355631) for 2 h. The pellet of small EVs was vigorously resuspended in 1 ml 1X PBS and ultracentrifuged at 49,000 rpm (100,000x g average) (TLA-100.3 Fixed-Angle Rotor, k-factor 59; Beckman Coulter Life Sciences) in polypropylene tubes (Beckman-Coulter Life Sciences, 357448) for 30 min.

The differential centrifugation protocol used for small EV concentration was scaled down using Beckman Coulter Life Sciences conversion calculator (https://www.mybeckman.ca/centrifuges/rotors/calculator) in order to perform the protocol identically but with less volume using the TLA-100.3 Fixed-Angle Rotor. The samples were centrifuged at 300x g average (2 min, k-factor 18800) and 2000x g average (2 min, k-factor 2800, FA-45-24-11 5424R, Eppendorf) before centrifugation at 10,000x g (15,000 rpm) (5 min, TLA-100.3, k-factor 633) and 100,000x g average (49,000 rpm, 30 min, k-factor 59, TLA-100.3). The pellet was vigorously resuspended in 1 ml 1X PBS and recentrifuged at 49,000 rpm (100,000x g average) (TLA-100.3 Fixed-Angle Rotor, k-factor 59, Beckman Coulter Life Sciences) in polypropylene tubes for another 30 min before analysis by Nanoparticle tracking or RNA extraction by TRIzol

4.5 | Fluorescence microscopy of siRNA and CD63

Fifty thousand HEK 293T cells were seeded on DPL-coated cover slips (Millipore Sigma, P7280-5MG). The cells were transfected with siGLO (Dharmacon, D-001610-01-05) at a 10 nM concentration in 1 ml of media using RNAiMAX, INTERFERin or JETPRIME as recommended for a well of a 12 well plate. Media was changed 24 h after transfection. Cells were fixed 6 and 48 h after transfection with 4% PFA in PBS for 10 min at room temperature. Cover slips were washed with 1X PBS thrice then stored at 4°C. Cover slips were washed twice with 1X PBS then incubated with 300 μl purified mouse antihuman CD63 antibody (1:100) (BD Pharmingen, 556019) in 1% BSA 0.25% Triton X-100 in 1X PBS overnight at 4°C in the dark. The following day, the cover slips were washed twice with 1X PBS then incubated with 300 μl goat anti-mouse Alexa 488 (1:500, Thermo Fisher Scientific, A11029) in 1% BSA 0.25% Triton X-100 in 1X PBS for 1 h at 4°C. Then, cover slips were washed twice with 1X PBS and mounted with VECTASHEILD solution (Vector Laboratories Inc, H-1200) and sealed. Images were acquired using a ZEISS Axio Imager 2 equipped with a 63X Plan-Apochromat 1.4 Oil lens, an AxioCam mRC detector and the ZEN 2.3 analysis software. Filter sets utilised include Blue (Excitation 390/22 nm, Emission 460/50 nm), Green (Excitation 470/20 nm, Emission 517/25 nm), and Red (Excitation 560/40 nm, Emission 690/50 nm).

4.6 | Flow cytometry

Cells were detached with trypsin and neutralised with culture media. The suspension was centrifuged at 300 xg for 5 min and the cell pellet was resuspended in 1% FBS in 1X PBS. The cell suspension was diluted to a concentration of 10^6 cells/ml, with a minimal volume of 500 μl, and filtered through a 40 μm sterile cell strainer (Thermo Fisher Scientific, 22-363-547) into 5 ml Falcon round-bottom polystyrene tubes (Thermo Fisher Scientific, 14-959-2A) prior to flow cytometry. GFP fluorescence was measured on a BD FACSCelesta Flow Cytometer or BD LSRFortessa Cell Analyser which were calibrated with untransfected HEK 293A GFP and HEK 293T controls. Ten thousand events were counted. Kaluza Flow Cytometry Analysis Software was used to gate the cells in order to exclude debris and cell clumps from analysis. Knockdown efficiency was evaluated by geometric mean fluorescence intensity (Geo MFI) percentage in relation to control samples of cells transfected with the associated reagent and scramble siRNA concentration.

4.7 | Nanoparticle tracking analysis

Nanoparticle Tracking Analysis (NTA) was performed on a ZetaView PMX-110. The ZetaView was calibrated upon each start-up using 102 nm polystyrene beads (Microtrac, 900383). Transfection complexes or precipitated small EVs were diluted in 1X PBS (1000X-1,000,000X) to be in the instrument's range for accurate measurement. Approximately 700 μl of the dilution was injected into the instrument. Once particle drift and concentration fell in acceptable ranges, video acquisition was performed

with the following settings: Sensitivity 85, Shutter Speed 40, Frame Rate (fps) 30, Resolution Highest, Camera Gain 770, Positions Measured 11, Minimum Brightness 15, Minimum Size (pixels) 10, Maximum Size (pixels) 500. Solutions in which sEV or transfection complexes were diluted were verified to have at least 100–1000-fold fewer particles than the sEV or transfection complex solutions.

4.8 | RNA isolation

A standard TRIzol extraction protocol was followed using 10 μg of glycogen (Thermo-Fisher Scientific, R0551 or AM9515) to facilitate precipitation of RNA. RNA was precipitated in isopropanol (0.5 mL per mL of TRIzol reagent), centrifuged at 13,500 rpm for 30 min at 4°C and washed with 75% nuclease-free ethanol (1 ml per ml of TRIzol reagent). The RNA pellet was then resuspended in 20 μl of nuclease-free water. Quantification and analysis was completed with Nanodrop 2000 spectrophotometer (Thermo Fisher Scientific, ND-2000) or a Synergy H1 Hybrid Multi–Mode plate reader (BioTek).

4.9 | Transfection

NSC-34 cells or HEK293 cells were grown to 60–80% confluence in antibiotic-free DMEM supplemented with 1% heat inactivated FBS prior to transfection. Transfections were performed according to the manufacturers' instructions using Lipofectamine RNAiMAX (Thermo Fisher Scientific, 13778150) and Opti-MEM (Thermo Fisher Scientific, 31985-070), INTERFERin (VWR, 89129–930), RiboJuice (Millipore Sigma, 71115-4) or electroporation. For example, for transfection in 15 cm plates (15 ml) 3.75×10^6 cells were seeded and transfection complexes were formed as follows: RNAiMAX (1125 μl Opti-MEM + 15 μl 10 μM siRNA + 67.5 μl RNAiMAX), INTERFERin (1.5 ml Opti-MEM + 15 μl 10 μM siRNA + 60 μl INTERFERin), and RiboJuice (1830 μl Opti-MEM + 15 μl 10 μM siRNA + 45 μl RiboJuice). For electroporation, cells were pelleted at 400x g for 5 min then resuspended in Opti-MEM prior to electroporation with a Gene Pulser Xcell Electroporation System (Bio-Rad, 1652661). The preprogrammed protocol for transfection of HEK 293 in a 2 mm cuvette was followed. However, voltage was doubled as the cuvette size used was 4 mm (Bio-Rad, 1652081). Electroporated samples were hastily transferred to prewarmed plated media. Six hours after transfection with all methods/reagents cell culture media was removed and cells were washed with 1X PBS. UltraCULTURE Serum-free Media (Lonza, BE12-725F) supplemented with 1% Penicillin-Streptomycin and 1% L-glutamine (Thermo Fisher Scientific, 25030–081) was added to the cells and conditioned media was collected for three consecutive days following. This media immediately underwent centrifugation at 300 g and 2000 g according to the sEV preparation protocol and then was stored at 4°C. The final steps of the sEV preparation protocol were performed on pooled conditioned media on day 3 post-transfection.

4.10 | RT-qPCR

MiScript II RT kit (Qiagen, 218161) was used to quantify siRNAs targeting GFP, SOD1, and alpha-synuclein as well as miRNAs. The manufacturer's miScript PCR system handbook was followed with the HiFlex buffer option but with 0.5 μl miScript Reverse Transcriptase Mix in a 20 μl reaction. cDNA (1 μl 1:6) was amplified using the miScript SYBR green PCR kit (Qiagen, 218076) and 10X miScript primer assays (5μM) (IDT, SOD1 siRNA 5′TTCAGTCAGTCCTTTAATGCTT3′, GFP siRNA 5′ ATGAACTTCAGGGTCAGCTTGC 3′, miR-106a – 5′ AAAAGTGCTTACAGTGCAGGTAG 3′, miR-15b – 5′ TAGCAGCACATCATGGTTTACA 3′) in accordance with the manufacturer's miScript PCR system handbook on a CFX384 or CFX96 Touch Real-Time PCR Detection System (Bio-Rad, 1855485 or 1855195) using a 10 μl reaction volume.

Copy number of siRNA per sEV was quantified as previously described (Reshke et al., 2020). In brief RT-qPCR was performed simultaneously on samples and a serial dilution of a known amount (6.25–13 fmol) of RT-qPCR product to generate a standard curve. C_q values of samples were plotted on the standard curve to determine the number of RNA molecules. As the RNA was prepared from a known number of small EVs (determined by Nanoparticle tracking analysis), the number of RNA molecules per sEV was calculated.

Primer annealing temperature was tested on pooled cDNA samples of transfection complexes and pooled samples of HEK 293T small EVs to ensure that the annealing temperature recommended by the manufacturer's protocol was in the primer's range of efficiency. Additionally, amplification of a serial dilution of these pooled samples helped determine the level of dilution (1:100) the cDNA should be diluted to be within the primer's efficiency range for qPCR. The steps are in accordance with MIQE guidelines.

For detection of alpha-synuclein mRNA, 100 or 500 ng of RNA isolated from cells was reverse transcribed with 50U M-MuLV reverse transcriptase (NEB, M0253L) using 100 uM Oligo(dT)18 primer and dNTP mix (ThermoFisher) in a 10 μl reaction. qPCR was performed with 2x GoTaq qPCR master mix (Promega) with the following primers: a-synuclein, CTTGCCTTCAAGC-

CTTCTGC and TCCTTGGTTTTGGAGCCTACAT, GAPDH AGGTCATCCCTGAGCTGAACG and GCCTGCTTCACCAC-CTTCTTG, and β-actin GGCATGGGTCAGAAGGATT and GGGGTGTTGAAGGTCTCAAA).

For quantification of SOD1 mRNA in primary mixed motor neurons from SOD1 G93A transgenic mice (Gurney et al., 1994), cultured as previously described (Reshke et al., 2020) Taqman Gene Expression Master Mix (Thermo Fisher Scientific, 4369510) and Taqman RNA Assays were used (Gusb - Mm01197698_m1; Pgk1 - Mm00435617_m1; Gapdh - Mm99999915_g1; SOD1 - Hs00533490_m1). Samples were amplified on a CFX384 or CFX96 Touch Real-Time PCR Detection System (Bio-Rad, 1855485 or 1855195) using a 10 μl reaction volume. Relative RNA levels were quantified using the DDCT method.

4.11 | Scanning electron microscopy

sEVs prepared by ultracentrifugation were fixed in 4% paraformaldehyde overnight and processed for scanning electron microscopy by the Nanoscale Biomedical Imaging Facility (SickKids Hospital, Toronto, Canada).

4.12 | Western blot

Cells or sEVs were lysed in ice-cold 0.1 M Tris (pH 7.4), 5 M NaCl, 0.5 M EDTA, 1% Triton-X 100 containing protease inhibitor cocktail. Protein concentration was measured using a Bradford Protein Assay (Biorad) or Micro BCA protein assay kit (Thermo Fisher, no. 23235). Samples were run on de-naturing SDS-PAGE gels in Laemmli loading buffer (50 mM Tris pH 6.8, 2% SDS, 10% glycerol, 5% β-mercaptoethanol, 0.1 M DTT) after heating at 99°C for 5 min. Proteins were transferred to polyvinylidene fluoride (PVDF) membranes, blocked with 5% milk in 1x TBST [10 mM Tris-HCl (pH 8), 150 mM NaCl, 0.05% Tween 20). The following antibodies were used : Flotillin-2 (C42A3 #3436S, New England Biolabs), Alix [3A9 #2171S, New England Biolabs], TSG101 [4A10, #GTX70255, Genetex), Syntenin-1 (Abcam #ab133267, clone EPR8102) and Tomm20 (Invitrogen #PA5-39247 polyclonal).

4.13 | Treatment of mixed motor neurons or SH-SY5Y cells with sEVs in dose responses

Primary cultures of mixed motor neurons were prepared from SOD1 G93A transgenic mice and treated with sEVs packaged with siRNA targeting human SOD1 as previously described (Reshke et al., 2020). SOD1 mRNA was quantified by RT-qPCR 3 days after treatment of cells with sEVs at the doses described. To normalize sEV doses to the amount of siRNA targeting SOD1 in each preparation, the relative amount of SOD1 siRNA was quantified by RT-qPCR using protocols described above. sEV doses were normalised to the relative amount of SOD1 siRNA in each preparation.

Human SH-SY5Y neuroblastoma cells were plated in a 24-well plate at a density of 5×10^4 cells per well (~50% confluence). After 24 h, differentiation was induced by lowering the FBS in culture media to 1% without antibiotics and adding 10 μM all transretinoic acid (RA) (Sigma-Aldrich Cat.no. R2625) at day 1, 4, and 7. sEV were prepared from HEK293 cells stably expressing pre-miR-451 backbones reprogrammed with siRNA targeting alpha-synuclein or GFP as previously described (Reshke et al., 2020). HEK293 cells were transfected or not according to the manufacturer's instructions and washed in PBS 6 h later. The following day cells were washed again with PBS and changed into Ultraculture media to begin sEV collection over the three following days as described above. At day 8 of differentiation of SH-SY5Y cells, sEV were added at a dose of 50×10^3 particles/ml, except in Figure 5i where additional doses of 10, 25, or 150×10^3 particles / ml were tested. Then, after 72 h of incubation with sEV, RNA was isolated from SH-SY5Y cells using TRIzol reagent. Levels of alpha-synuclein mRNA was measured by RT-qPCR normalizing to reference mRNAs (GAPDH and Beta-Actin) using M-MuLV Reverse Transcriptase (NEB, M0253L) and GoTaq® qPCR Master Mix (Promega, A6002).

4.14 | Analysis of lipidome of RNAiMax transfection complexes and sEVs

Untargeted LC-MS lipidomic analysis was performed by the Metabolomics Innovation Centre (TMIC, University of Alberta, Canada). Three independent samples of RNAiMAX transfection complexes, sEV or sEV from cells transfected with RNAiMAX were processed for lipidomic analysis. In brief, samples were extracted with a modified Folch method. Aliquots of 60.0 ml of each sample were vortexed with 1.4 ml of a mixture of deuterated lipids employed as internal standards and 400 ml of methanol. The mixture was extracted with 799 ml of dichloromethane and 240 ml of water. After 10 min equilibration at room temperature, samples were centrifuged at 16,000 g for 10 min at 4 C. Part of the organic layer was evaporated with nitrogen and resuspended in mobile phases before LC-MS analysis. Samples were analysed on a Thermo Vanquish UHPLC linked to a Bruker Impact II QTOF using a Waters Acquity CSH C18 column with a mass range of 150–1500 m/z under positive and negative ionization. Lipid features were extracted and processed with a mass tolerance of 5 mDa. Lipids were identified by MS/MS spectral match (MS/MS

score ≥500 (tier 1) or ≥100 (tier 2), precursor m/z tolerance of 5.0 mDa and lipid class-based retention time filter) or mass match (m/z tolerance of 5.0 mDa and a 6-tier filtering and scoring approach to refine identifications). After identification, the peak intensities were normalised by one of 15 deuterated lipids employed as internal standards based on lipid class similarity. The obtained intensity ratios were filtered by relative standard deviation (RSD) of quality control experimental replicates (RSD ≤30%). Noninformative features (i.e., internal standards and features with near-constant values between the groups determined by low RSD) were also removed before auto-scaling, normalization to the median value and statistical analysis employing MetaboAnalyst 5.0 (Zardini Buzatto et al., 2021; Zardini Buzatto et al., 2021).

4.15 | Optiprep gradients

Optiprep gradients were performed according to the protocol previously described. Briefly, sEVs pellets were resuspended in 3 ml PBS, to which 9 ml of 60% iodixanol (Optiprep) was added. This solution was added to the bottom of an ultracentrifuge tube. Iodixanol solutions of 30%, 23%, 18% were layered on top and the tube was ultracentrifuged for 16 h at 150,000 x g (maximum) in a SW32 Ti swinging bucket rotor (Beckman-Coulter, k-factor 239). Twelve fractions were collected. Density was measured using a refractometer. Half of each fraction was set aside for RNA purification using TRIzol LS for RT-qPCR. The other half of fractions was ultracentrifuged to pellet sEVs for analysis by Western blot.

4.16 | Knockdown by sEVs and transfection complexes isolated by Optiprep density gradient

3×10^6 wild-type HEK293 cells or stable HEK293 cells expressing SOD1 siRNA in the pre-miR-451 backbone were plated into 15 cm plates containing 15 ml of complete DMEM. The next day, plates were transfected with RNAiMAx as described above. Four hours after transfection, plates were washed three times in PBS and media was replaced with sEV-depleted complete DMEM. Conditioned media was then centrifuged at 300 xg and 200 xg for 10 min each and filtered through a 0.22um filter (Thermo-Scientific, catalogue no. 09–741–04). Filtered media was then concentrated to ~8 ml using the KR2i tangential flow filtration system (Repligen) with a 20 cm^2 modified polyethersulfone hollow fibre column with 500 kDa cut-off (Repligen, C02-E500-05-S) at a flow rate of 30 ml min^{-1} with transmembrane pressure of 3.0 PSI to achieve a shear rate of 2000 s^{-1}. Concentrated media underwent 5x buffer exchange in PlasmaLyte solution (Baxter, JB2544). One ml of TFF isolated sEVs was then separated on an iodixanol gradient, as described herein. Additionally, RNAimax transfection complexes were prepared with volumes required for transfecting three 15 cm plates and loaded directly onto gradients. One ml fractions were collected from the top of each gradient. Fractions 1 and 2 enriched in RNAiMax transfection complexes, were collected together, as were fractions 3 and 4, enriched in sEV markers. Particles in each set of fractions were quantified using NTA (as above). Wild-type HEK293 cells were then treated with 20,000 particles/cell from fractions 1 and 2 or 100,000 particles/cell from fractions 3 and 4. Knockdown of SOD1 was measured 48 h later. 0.5 ml of the gradient fractions were diluted in 29 ml of PBS and ultracentrifuged at 100,000xg for 2 h in a SW32 rotor (Beckman-Coulter Life Sciences). Pellets were lysed and prepared for Western Blot as described herein.

4.17 | Flow cytometry using annexin V and propidium iodide staining

HEK293 cells were plate at 2×10^5 cell/well using six well plates. Cells were transfected with control siRNA using either INTERFERin® or RNAiMAX according to the manufacturer's protocol, negative controls were cells incubated with diluent for the transfection reagent following the same procedures. Cells were collected after 72 h, each sample was resuspended in 100 ml Annexin V binding buffer (10 mM HEPES pH 7.4, 140 mM NaCl and 2.5 mM $CaCl_2$). Either 5 ml of Alexa Fluor™ 488 conjugate (ThermoFisher, A13201) and/or 10 mg/ml Propidium iodide (PI, ThermoFisher, V13244) were added into samples and samples were incubated in the dark at room temperature for 15 min. Flow cytometry was performed using a Becton Dickinson Celesta.

4.18 | Image quantification

Pearson's coefficient was generated using the JACoP plugin in Image J. Threshold were set identically for all images and a particle size of 20-infinity was used. Images focused on the nuclei of healthy cells were randomly acquired and quantified, using identical thresholds and microscope settings.

4.19 | Effect of pH on sEV and RNAiMax transfection complexes

sEVs, RNAiMax complexes or a 1 particle:1 particle mixture of the two were analysed by Nanoparticle tracking analysis in 1 ml of PBS whose pH had been adjusted to pH 7.2, 6.5 or 5.5. For immediate readings, 1 ml of samples was diluted in 1 ml of PBS (at pH7, 6.5 or 5.5) and injected into the instrument immediately and the readings were recorded as soon as the drift was in the acceptable range (usually 1–2 min). Incubations for 1 h were performed 37°C.

ACKNOWLEDGEMENT

This work was funded by a Discovery Grant and Discovery Grant Accelerator from the Natural Science and Engineering Research Council of Canada (DG).

CONFLICT OF INTEREST

The authors declare that they have no conflict of interest.

AUTHOR CONTRIBUTIONS

Carmen Daniela Sosa-Miranda performed fluorescent microscopy and all experiments involving delivery of siRNA targeting alpha-synuclein by sEV. James A. Taylor performed Western blot and RT-qPCR of miRNAs in 293 cells either untreated or transfected. Ryan Reshke performed analyses of sEV and transfection complexes alone and co-incubated in the absence of cells. Alexandre Savard performed experiments measuring sEV and transfection complex effects on primary mixed motor neuron cultures. Huishan Guo performed dose-response of sEV delivery on SH-SY5Y cells and Nanoparticle tracking analysis of sEV at different pHs. Ryan Reshke performed Optiprep gradients, except RT-qPCR (James A. Taylor). Jenna McCann performed all other experiments. Derrick J. Gibbings conceived and designed the research and wrote the paper with assistance from James A. Taylor and Jenna McCann.

REFERENCES

Adams, D., Gonzalez-Duarte, A., O'riordan, W. D., Yang, C. -. C., Ueda, M., Kristen, A. V., Tournev, I., Schmidt, H. H., Coelho, T., Berk, J. L., Lin, K. -. P., Vita, G., Attarian, S., Planté-Bordeneuve, V., Mezei, M. M., Campistol, J. M., Buades, J., Brannagan, T. H., Kim, B. J., & Suhr, O. B. (2018). Patisiran, an RNAi therapeutic, for hereditary transthyretin amyloidosis. *New England Journal of Medicine*, *379*, 11–21. https://doi.org/10.1056/NEJMoa1716153

Akinc, A., & Battaglia, G. (2013). Exploiting endocytosis for nanomedicines. *Cold Spring Harbor Perspectives in Biology*, *5*, a016980.

Akinc, A., Querbes, W., De, S., Qin, J., Frank-Kamenetsky, M., Jayaprakash, K. N., & Maier, M. A. (2010). Targeted delivery of RNAi therapeutics with endogenous and exogenous ligand-based mechanisms. *Molecular Therapy : The Journal of the American Society of Gene Therapy*, *18*, 1357–1364.

Alvarez-Erviti, L., Seow, Y., Yin, H., Betts, C., Lakhal, S., & Wood, M. J. A. (2011). Delivery of siRNA to the mouse brain by systemic injection of targeted exosomes. *Nature Biotechnology*, *29*, 341–345.

Balwani, M., Sardh, E., Ventura, P., Peiró, P. A., Rees, D. C., Stölzel, U., & Gouya, L., ENVISION Investigators. (2020). Phase 3 trial of RNAi therapeutic givosiran for acute intermittent porphyria. *The New England Journal of Medicine*, *382*, 2289–2301.

Behzadi, S., Serpooshan, V., Tao, W., Hamaly, M. A., Alkawareek, M. Y., Dreaden, E. C., Brown, D., Alkilany, A. M., Farokhzad, O. C., & Mahmoudi, M. (2017). Cellular uptake of nanoparticles: Journey inside the cell. *Chemical Society Reviews*, *46*, 4218–4244.

Booth, A. M., Fang, Yi., Fallon, J. K., Yang, M.Jr., Hildreth, J. E. K., & Gould, S. J. (2006). Exosomes and HIV Gag bud from endosome-like domains of the T cell plasma membrane. *Journal of Cell Biology*, *172*, 923–935. https://doi.org/10.1083/jcb.200508014

Brown, C. R., Gupta, S., Qin, J., Racie, T., He, G., Lentini, S., Malone, R., Yu, M., Matsuda, S., Shulga-Morskaya, S., Nair, A. V., Theile, C. S., Schmidt, K., Shahraz, A., Goel, V., Parmar, R. G., Zlatev, I., Schlegel, M. K., Nair, J. K., & Jadhav, V. (2020). Investigating the pharmacodynamic durability of GalNAc–siRNA conjugates. *Nucleic Acids Research*, *48*, 11827.

Busatto, S., Iannotta, D., Walker, S. A., Di Marzio, L., & Wolfram, J. (2021). A simple and quick method for loading proteins in extracellular vesicles. *Pharmaceuticals*, *14*, 356.

Caffrey, D. R., Zhao, J., Song, Z., Schaffer, M. E., Haney, S. A., Subramanian, R. R., Seymour, A. B., & Hughes, J. D. (2011). siRNA off-target effects can be reduced at concentrations that match their individual potency. *Plos One*, *6*, e21503.

Chevillet, J. R., Kang, Q., Ruf, I. K., Briggs, H. A., Vojtech, L. N., Hughes, S. M., Cheng, H. H., Arroyo, J. D., Meredith, E. K., Gallichotte, E. N., Pogosova-Agadjanyan, E. L., Morrissey, C., Stirewalt, D. L., Hladik, F., Yu, E. Y., Higano, C. S., & Tewari, M. (2014). Quantitative and stoichiometric analysis of the microRNA content of exosomes. *Proceedings of the National Academy of Sciences*, *111*, 14888–14893.

Didiot, M. -. C., Hall, L. M., Coles, A. H., Haraszti, R. A., Godinho, B. M., Chase, K., Sapp, E., Ly, S., Alterman, J. F., Hassler, M. R., Echeverria, D., Raj, L., Morrissey, D. V., Difiglia, M., Aronin, N., & Khvorova, A. (2016). Exosome-mediated delivery of hydrophobically modified siRNA for Huntingtin mRNA silencing. *Molecular Therapy*, *24*, 1836–1847. https://doi.org/10.1038/mt.2016.126

Dowdy, S. F. (2017). Overcoming cellular barriers for RNA therapeutics. *Nature Biotechnology*, *35*, 222–229.

Du Rietz, H., Hedlund, H., Wilhelmson, S., Nordenfelt, P., & Wittrup, A. (2020). Imaging small molecule-induced endosomal escape of siRNA. *Nature Communications*, *11*, 1–17.

Evers, M. J. W., Wakker, S. I., Groot, E. M., Jong, O. G., Gitz-François, J. J. J., Seinen, C. S., Sluijter, J. P. G., Schiffelers, R. M., & Vader, P. (2021). Functional siRNA delivery by extracellular vesicle-liposome hybrid nanoparticles. *Advanced Healthcare Materials*, *11*, 2101202. https://doi.org/10.1002/ADHM.202101202

Fire, A., Xu, S., Montgomery, M. K., Kostas, S. A., Driver, S. E., & Mello, C. C. (1998). Potent and specific genetic interference by double-stranded RNA in caenorhabditis elegans. *Nature*, *391*, 806–811. https://doi.org/10.1038/35888

Gilleron, J., Paramasivam, P., Zeigerer, A., Querbes, W., Marsico, G., Andree, C., Seifert, S., Amaya, P., Stöter, M., Koteliansky, V., Waldmann, H., Fitzgerald, K., Kalaidzidis, Y., Akinc, A., Maier, M. A., Manoharan, M., Bickle, M., & Zerial, M. (2015). Identification of siRNA delivery enhancers by a chemical library screen. *Nucleic Acids Research*, *43*, 7984–8001.

Gilleron, J., Querbes, W., Zeigerer, A., Borodovsky, A., Marsico, G., Schubert, U., Manygoats, K., Seifert, S., Andree, C., Stöter, M., Epstein-Barash, H., Zhang, L., Koteliansky, V., Fitzgerald, K., Fava, E., Bickle, M., Kalaidzidis, Y., Akinc, A., Maier, M., & Zerial, M. (2013). Image-based analysis of lipid nanoparticle–mediated siRNA delivery, intracellular trafficking and endosomal escape. *Nature Biotechnology*, *31*, 638–646.

Gillmore, J. D., Gane, E. d., Taubel, J., Kao, J. J., Fontana, M., Maitland, M. L., & Lebwohl, D. (2021). CRISPR-Cas9 in vivo gene editing for transthyretin amyloidosis. *The New England Journal of Medicine*, *385*, 493–502.

Gurney, M. E., Pu, H., Chiu, A. Y., Dal Canto, M. C., Polchow, C. Y., Alexander, D. D., Caliendo, J., Hentati, A., Kwon, Y. W., Deng, H. -. X., Chen, W., Zhai, P., Sufit, R. L., & Siddique, T. (1994). Motor neuron degeneration in mice that express a human Cu, Zn superoxide dismutase mutation. *Science*, *264*, 1772–1775. https://doi.org/10.1126/science.8209258

Hou, X., Zaks, T., Langer, R., & Dong, Y. (2021). Lipid nanoparticles for mRNA delivery. *Nature Reviews. Materials*, *1*, 1078–1094. https://doi.org/10.1038/S41578-021-00358-0

Hui, S. W., Langner, M., Zhao, Y. L., Ross, P., Hurley, E., & Chan, K. (1996). The role of helper lipids in cationic liposome-mediated gene transfer. *Biophysical Journal*, *71*, 590–599.

Jeppesen, D. K., Fenix, A. M., Franklin, J. L., Higginbotham, J. N., Zhang, Q., Zimmerman, L. J., Liebler, D. C., Ping, J., Liu, Q. i., Evans, R., Fissell, W. H., Patton, J. G., Rome, L. H., Burnette, D. T., & Coffey, R. J. (2019). Reassessment of exosome composition. *Cell*, *177*, 428–445. e18.

Jonker, C., deHeus, C., Faber, L., Brink, C. T., Potze, L., Fermie, J., Liv, N., & Klumperman, J. (2017). An adapted protocol to overcome endosomal damage caused by polyethylenimine (PEI) mediated transfections. *Matters*, *3*, e201711000012.

Joshi, B. S., De Beer, M. A., Giepmans, B. N. G., & Zuhorn, I. S. (2020). Endocytosis of extracellular vesicles and release of their cargo from endosomes. *ACS Nano*, *14*, 4444–4455.

Kamerkar, S., Lebleu, V. S., Sugimoto, H., Yang, S., Ruivo, C. F., Melo, S. A., Lee, J. J., & Kalluri, R. (2017). Exosomes facilitate therapeutic targeting of oncogenic KRAS in pancreatic cancer. *Nature*, *546*, 498–503. https://doi.org/10.1038/nature22341

Kanasty, R., Dorkin, J. R., Vegas, A., & Anderson, D. (2013). Delivery materials for siRNA therapeutics. *Nature Materials*, *12*, 967–977.

Kanasty, R. L., Whitehead, K. A., Vegas, A. J., & Anderson, D. G. (2012). Action and reaction: The biological response to siRNA and its delivery vehicles. *Molecular Therapy : The Journal of the American Society of Gene Therapy*, *20*, 513–524.

Kichler, A., Leborgne, C., Coeytaux, E., & Danos, O. (2001). Polyethylenimine-mediated gene delivery: A mechanistic study. *The Journal of Gene Medicine*, *3*, 135–144.

Kim, M., Jeong, M., Hur, S., Cho, Y., Park, J., Jung, H., Seo, Y., Woo, H. A., Nam, K. T., Lee, K., & Lee, H. (2021). Engineered ionizable lipid nanoparticles for targeted delivery of RNA therapeutics into different types of cells in the liver. *Science Advances*, *7*, eabf4398.

Klein, D., Goldberg, S., Theile, C. S., Dambra, R., Haskell, K., Kuhar, E., Lin, T., Parmar, R., Manoharan, M., Richter, M., Wu, M., Zarazowski, J. M., Jadhav, V., Maier, M. A., Sepp-Lorenzino, L., O'Neil, K., & Dudkin, V. (2021). Centyrin ligands for extrahepatic delivery of siRNA. *Molecular Therapy : The Journal of the American Society of Gene Therapy*, *29*, 2053–2066.

Kojima, R., Bojar, D., Rizzi, G., Hamri, G. C.-El, El-Baba, M. D., Saxena, P., Ausländer, S., Tan, K. R., & Fussenegger, M. (2018). Designer exosomes produced by implanted cells intracerebrally deliver therapeutic cargo for Parkinson's disease treatment. *Nature Communications*, *9*, 1–10.

Kooijmans, S. A. A., Stremersch, S., Braeckmans, K., De Smedt, S. C., Hendrix, A. n., Wood, M. J. A., Schiffelers, R. M., Raemdonck, K., & Vader, P. (2013). Electroporation-induced siRNA precipitation obscures the efficiency of siRNA loading into extracellular vesicles. *Journal of Controlled Release*, *172*, 229–238.

Kulkarni, J. A., Darjuan, M. M., Mercer, J. E., Chen, S., Van Der Meel, R., Thewalt, J. L., Tam, Y. Y. i. C., & Cullis, P. R. (2018). On the formation and morphology of lipid nanoparticles containing ionizable cationic lipids and siRNA. *ACS Nano*, *12*, 4787–4795.

Lamparski, H. G., Metha-Damani, A., Yao, J. -. Y., Patel, S., Hsu, Di. -. H., Ruegg, C., & Le Pecq, J. -. B. (2002). Production and characterization of clinical grade exosomes derived from dendritic cells. *Journal of Immunological Methods*, *270*, 211–226.

Liu, L., & Chen, X. (2018). Intercellular and systemic trafficking of RNAs in plants. *Nature Plants*, *4*, 869–878. https://doi.org/10.1038/s41477-018-0288-5

Liu, Z., Wang, S., Tapeinos, C., Torrieri, G., Känkänen, V., El-Sayed, N., Python, A., Hirvonen, J. T., & Santos, H. A. (2021). Non-viral nanoparticles for RNA interference: Principles of design and practical guidelines. *Advanced Drug Delivery Reviews*, *174*, 576–612. https://doi.org/10.1016/j.addr.2021.05.018

Love, K. T., Mahon, K. P., Levins, C. G., Whitehead, K. A., Querbes, W., Dorkin, J. R., Qin, J., Cantley, W., Qin, L. L., Racie, T., Frank-Kamenetsky, M., Yip, KaN., Alvarez, R., Sah, D. W. Y., De Fougerolles, A., Fitzgerald, K., Koteliansky, V., Akinc, A., Langer, R., & Anderson, D. G. (2010). Lipid-like materials for low-dose, in vivo gene silencing. *Proceedings of the National Academy of Sciences*, *107*, 1864–1869. https://doi.org/10.1073/pnas.0910603106

Luga, V., Zhang, L., Viloria-Petit, A. M., Ogunjimi, A. A., Inanlou, M. R., Chiu, E., Buchanan, M., Hosein, A. N., Basik, M., & Wrana, J. L. (2012). Exosomes mediate stromal mobilization of autocrine Wnt-PCP signaling in breast cancer cell migration. *Cell*, *151*, 1542–1556. https://doi.org/10.1016/j.cell.2012.11.024

Mateescu, B., Kowal, E. J. K., Van Balkom, B. W. M., Bartel, S., Bhattacharyya, S. N., Buzás, E. I., Buck, A. H., De Candia, P., Chow, F. W. N., Das, S., Driedonks, T. A. P., Fernández-Messina, L., Haderk, F., Hill, A. F., Jones, J. C., Van Keuren-Jensen, K. R., Lai, C. P., Lässer, C., Di Liegro, I., & Nolte-'t Hoen, E. N. M. (2017). Obstacles and opportunities in the functional analysis of extracellular vesicle RNA - An ISEV position paper. *Journal of Extracellular Vesicles*, *6*, 1286095. https://doi.org/10.1080/20013078.2017.1286095

Maugeri, M., Nawaz, M., Papadimitriou, A., Angerfors, A., Camponeschi, A., Na, M., Hölttä, M., Skantze, P., Johansson, S., Sundqvist, M., Lindquist, J., Kjellman, T., Mårtensson, I. -. L., Jin, T., Sunnerhagen, P., Östman, S., Lindfors, L., & Valadi, H. (2019). Linkage between endosomal escape of LNP-mRNA and loading into EVs for transport to other cells. *Nature Communications*, *10*, 1–15.

Mihaila, R., Chang, S., Wei, A. T., Hu, Z. Y., Ruhela, D., Shadel, T. R., Duenwald, S., Payson, E., Cunningham, J. J., Kuklin, N., & Mathre, D. J. (2011). Lipid nanoparticle purification by Spin Centrifugation-Dialysis (SCD): A facile and high-throughput approach for small scale preparation of siRNA-lipid complexes. *International Journal of Pharmaceutics*, *420*, 118–121.

Mok, K. W., & Cullis, P. R. (1997). Structural and fusogenic properties of cationic liposomes in the presence of plasmid DNA. *Biophysical Journal*, *73*, 2534–2545.

Muller, L., Hong, C. -. S., Stolz, D. B., Watkins, S. C., & Whiteside, T. L. (2014). Isolation of biologically-active exosomes from human plasma. *Journal of Immunological Methods*, *411*, 55–65.

Murphy, D. E., De Jong, O. G., Evers, M. J. W., Nurazizah, M., Schiffelers, R. M., & Vader, P. (2021). Natural or synthetic RNA delivery: A stoichiometric comparison of extracellular vesicles and synthetic nanoparticles. *Nano Letters*, *21*, 1888–1895.

Ogris, M., Steinlein, P., Kursa, M., Mechtler, K., Kircheis, R., & Wagner, E. (1998). The size of DNA/transferrin-PEI complexes is an important factor for gene expression in cultured cells. *Gene Therapy*, *5*, 1425–1433.

Ohno, S. -. I., Takanashi, M., Sudo, K., Ueda, S., Ishikawa, A., Matsuyama, N., Fujita, K., Mizutani, T., Ohgi, T., Ochiya, T., Gotoh, N., & Kuroda, M. (2012). Systemically injected exosomes targeted to EGFR deliver antitumor MicroRNA to breast cancer cells. *Molecular Therapy*, *21*, 185–191.

Pei, Yi., Hancock, P. J., Zhang, H., Bartz, R., Cherrin, C., Innocent, N., Pomerantz, C. J., Seitzer, J., Koser, M. L., Abrams, M. T., Xu, Y., Kuklin, N. A., Burke, P. A., Sachs, A. B., Sepp-Lorenzino, L., & Barnett, S. F. (2010). Quantitative evaluation of siRNA delivery in vivo. *RNA*, *16*, 2553–2563.

Piffoux, M., Silva, A. K. A., Wilhelm, C., Gazeau, F., & Tareste, D. (2018). Modification of extracellular vesicles by fusion with liposomes for the design of personalized biogenic drug delivery systems. *ACS Nano*, *12*, 6830–6842. (2018).

Piotrowski-Daspit, A. S., Kauffman, A. C., Bracaglia, L. G., & Saltzman, W. M. (2020). Polymeric vehicles for nucleic acid delivery. *Advanced Drug Delivery Reviews*, *156*, 119.

Rehman, Z. U. r., Hoekstra, D., & Zuhorn, I. S. (2013). Mechanism of polyplex- and lipoplex-mediated delivery of nucleic acids: Real-time visualization of transient membrane destabilization without endosomal lysis. *ACS Nano*, *7*, 3767–3777.

Reshke, R., Taylor, J. A., Savard, A., Guo, H., Rhym, L. H., Kowalski, P. S., Trung, MyT., Campbell, C., Little, W., Anderson, D. G., & Gibbings, D. (2020). Reduction of the therapeutic dose of silencing RNA by packaging it in extracellular vesicles via a pre-microRNA backbone. *Nature Biomedical Engineering*, *4*, 52–68. https://doi.org/10.1038/s41551-019-0502-4

Ridder, K., Sevko, A., Heide, J., Dams, M., Rupp, A. -. K., Macas, J., Starmann, J., Tjwa, M., Plate, K. H., Sültmann, H., Altevogt, P., Umansky, V., & Momma, S. (2015). Extracellular vesicle-mediated transfer of functional RNA in the tumor microenvironment. *Oncoimmunology*, *4*, e1008371.

Sahay, G., Querbes, W., Alabi, C., Eltoukhy, A., Sarkar, S., Zurenko, C., Karagiannis, E., Love, K., Chen, D., Zoncu, R., Buganim, Y., Schroeder, A., Langer, R., & Anderson, D. G. (2013). Efficiency of siRNA delivery by lipid nanoparticles is limited by endocytic recycling. *Nature Biotechnology*, *31*, 653–658.

Sahay, G., Querbes, W., Alabi, C., Eltoukhy, A., Sarkar, S., Zurenko, C., Karagiannis, E., Love, K., Chen, D., Zoncu, R., Buganim, Y., Schroeder, A., Langer, R., & Anderson, D. G. (2013). Efficiency of siRNA delivery by lipid nanoparticles is limited by endocytic recycling. *Nature Biotechnology*, *31*, 653–658. https://doi.org/10.1038/nbt.2614

Sato, Y. T., Umezaki, K., Sawada, S., Mukai, S. -. a., Sasaki, Y., Harada, N., Shiku, H., & Akiyoshi, K. (2016). Engineering hybrid exosomes by membrane fusion with liposomes. *Scientific Reports*, *6*, 1–11.

Sayers, E. J., Peel, S. E., Schantz, A., England, R. M., Beano, M., Bates, S. M., Desai, A. S., Puri, S., Ashford, M. B., & Jones, A. T. (2019). Endocytic profiling of cancer cell models reveals critical factors influencing LNP-mediated mRNA delivery and protein expression. *Molecular Therapy*, *27*, 1950–1962.

Selby, L. I., Cortez-Jugo, C. M., Such, G. K., & Johnston, A. P. R. (2017). Nanoescapology: Progress toward understanding the endosomal escape of polymeric nanoparticles. *Wiley Interdisciplinary Reviews. Nanomedicine and Nanobiotechnology*, *9*, e1452.

Shtam, T. A., Kovalev, R. A., Varfolomeeva, E. Y. u., Makarov, E. M., Kil, Y. V., & Filatov, M. V. (2013). Exosomes are natural carriers of exogenous siRNA to human cells in vitro. *Cell Communication and Signaling*, *11*, 1–10.

Skog, J., Würdinger, T., Van Rijn, S., Meijer, D. H., Gainche, L., Curry, W. T., Carter, B. S., Krichevsky, A. M., & Breakefield, X. O. (2008). Glioblastoma microvesicles transport RNA and proteins that promote tumour growth and provide diagnostic biomarkers. *Nature Cell Biology*, *10*, 1470–1476.

Sork, H., Nordin, J. Z., Turunen, J. J., Wiklander, O. P. b., Bestas, B., Zaghloul, E. M., Margus, H., Padari, K., Duru, A. D., Corso, G., Bost, J., Vader, P., Pooga, M., Smith, C. i. E., Wood, M. J. a., Schiffelers, R. M., Hällbrink, M., & Andaloussi, S. E. l. (2016). Lipid-based transfection reagents exhibit cryo-induced increase in transfection efficiency. *Molecular Therapy - Nucleic Acids*, *5*, e290.

Stewart, M. P., Sharei, A., Ding, X., Sahay, G., Langer, R., & Jensen, K. F. (2016). In vitro and ex vivo strategies for intracellular delivery. *Nature*, *538*, 183–192. https://doi.org/10.1038/nature19764

Takov, K., Yellon, D. M., & Davidson, S. M. (2017). Confounding factors in vesicle uptake studies using fluorescent lipophilic membrane dyes. *Journal of Extracellular Vesicles*, *6*, 1388731.

Théry, C., Witwer, K. W., Aikawa, E., Alcaraz, M. J., Anderson, J. D., Andriantsitohaina, R., Antoniou, A., Arab, T., Archer, F., Atkin-Smith, G. K., Ayre, D. C., Bach, J. -. M., Bachurski, D., Baharvand, H., Balaj, L., Baldacchino, S., Bauer, N. N., Baxter, A. A., Bebawy, M., & Zuba-Surma, E. K. (2018). Minimal information for studies of extracellular vesicles 2018 (MISEV2018): A position statement of the International Society for Extracellular Vesicles and update of the MISEV2014 guidelines. *Journal of Extracellular Vesicles*, *7*, 1535750. https://doi.org/10.1080/20013078.2018.1535750

Usman, W. M., Pham, T. C., Kwok, Y. Y., Vu, L. T., Ma, V., Peng, B., Chan, Y. S., Wei, L., Chin, S. M., Azad, A., He, A. B. -. L., Leung, A. Y. H., Yang, M., Shyh-Chang, N. g., Cho, W. C., Shi, J., & Le, M. T. N. (2018). Efficient RNA drug delivery using red blood cell extracellular vesicles. *Nature Communications*, *9*, 1–15.

Valadi, H., Ekström, K., Bossios, A., Sjöstrand, M., Lee, J. J., & Lötvall, J. O. (2007). Exosome-mediated transfer of mRNAs and microRNAs is a novel mechanism of genetic exchange between cells. *Nature Cell Biology*, *9*, 654–659.

Van De Vyver, T., Bogaert, B., De Backer, L., Joris, F., Guagliardo, R., Van Hoeck, J., Merckx, P., Van Calenbergh, S., Ramishetti, S., Peer, D., Remaut, K., De Smedt, S. C., & Raemdonck, K. (2020). Cationic amphiphilic drugs boost the lysosomal escape of small nucleic acid therapeutics in a nanocarrier-dependent manner. *ACS Nano*, *14*, 4774–4791.

Van Niel, G., D'angelo, G., & Raposo, G. (2018). Shedding light on the cell biology of extracellular vesicles. *Nature Reviews Molecular Cell Biology*, *19*, 213–228.

Wang, Q., Yu, J., Kadungure, T., Beyene, J., Zhang, H., & Lu, Q. (2018). ARMMs as a versatile platform for intracellular delivery of macromolecules. *Nature Communications*, *9*, 1–7.

Wheeler, J. J., Palmer, L., Ossanlou, M., Maclachlan, I., Graham, R. W., Zhang, Y. P., Hope, M. J., Scherrer, P., & Cullis, P. R. (1999). Stabilized plasmid-lipid particles: Construction and characterization. *Gene Therapy*, *6*, 271–281.

Whitehead, K. A., Dorkin, J. R., Vegas, A. J., Chang, P. H., Veiseh, O., Matthews, J., Fenton, O. S., Zhang, Y., Olejnik, K. T., Yesilyurt, V., Chen, D., Barros, S., Klebanov, B., Novobrantseva, T., Langer, R., & Anderson, D. G. (2014). Degradable lipid nanoparticles with predictable in vivo siRNA delivery activity. *Nature Communications*, *5*, 1–10.

Wittrup, A., Ai, A., Liu, X., Hamar, P., Trifonova, R., Charisse, K., Manoharan, M., Kirchhausen, T., & Lieberman, J. (2015). Visualizing lipid-formulated siRNA release from endosomes and target gene knockdown. *Nature Biotechnology*, *33*, 870–876.

Zardini Buzatto, A., Abdel Jabar, M., Nizami, I., Dasouki, M., Li, L., & Abdel Rahman, A. M. (2021). Lipidome alterations induced by cystic fibrosis, CFTR mutation, and lung function. *Journal of Proteome Research*, *20*, 549–564.

Zardini Buzatto, A., Tatlay, J., Bajwa, B., Mung, D., Camicioli, R., Dixon, R. A., & Li, L. (2021). Comprehensive serum lipidomics for detecting incipient dementia in Parkinson's disease. *Journal of Proteome Research*, *20*, 4053–4067.

Zelphati, O., & Szoka, F. C.Jr. (1996). Intracellular distribution and mechanism of delivery of oligonucleotides mediated by cationic lipids. *Pharmaceutical Research*, *13*, 1367–1372.

SUPPORTING INFORMATION

Additional supporting information may be found in the online version of the article at the publisher's website.

How to cite this article: McCann, J., Sosa-Miranda, C. D., Guo, H., Reshke, R., Savard, A., Zardini Buzatto, A., Taylor, J. A., Li, L., & Gibbings, D. J. (2022). Contaminating transfection complexes can masquerade as small extracellular vesicles and impair their delivery of RNA. *Journal of Extracellular Vesicles*, *11,* e12220. https://doi.org/10.1002/jev2.12220